Paper 25

Mineral Exploration Using Natural EM Fields

Jansen, J.C. [1], Cristall, J.A. [1]

1. Anglo American plc

ABSTRACT

The understanding of the geological processes behind the formation of mineral systems has advanced remarkably over the past two decades and has initiated a re-think with respect to the optimal geophysical methods required to both target and delineate economic ore bodies. The mineral system concept of McCuaig and Hronsky (2014) proposes four critical elements that must combine in various scales over space and time: whole lithosphere architecture, transient favourable geodynamics, fertility, and preservation of the primary depositional zone. They conclude that "[the mineral system concept] focuses mineral exploration strategies on incorporating primary datasets that can map the critical elements of mineral systems at a variety of scales, and particularly the regional to camp scales needed to make exploration decisions."

With exploration evolving to take a holistic view of the complete mineral system in targeting, geophysics has adapted to making greater use of techniques that can explore scales ranging from deposit to lithospheric. While the geophysical toolbox is filled with many techniques, only a few of them are capable of the depth investigation required to expand our view past the deposit scale: active- and passive-seismics, and methods that make use of Earth's natural gravitational, magnetic, and electromagnetic (EM) fields. Gravity and magnetics are ubiquitous in datasets ranging from continental to prospect scales and the use of seismic techniques in mineral exploration is growing. But nothing compares to natural field EM methods if the goal is 3D conductivity imaging to kilometres depth combined with ease of data collection. Over the past decade, these have become mainstream in mineral exploration, and recent advances in the joint inversion of ground and airborne data are making natural field EM methods an even more powerful tool for resolving complete mineral systems.

Examples of natural field EM techniques applied to a variety of mineral systems over the past decade are presented, beginning with a crustal scale magnetotelluric transect across the Gawler Craton and the super-giant Olympic Dam IOCG deposit of South Australia, and followed by illustrations from porphyry systems (Collahuasi, Pebble, El Salvador, Los Bronces, Cobre Panama, Resolution, Santa Cecilia, and Morrison) that dominate this paper owing to the economic significance of porphyry copper-gold deposits globally and because of their amenability to large-scale conductivity imaging. Further applications to sedimentary copper (Frontier and Kansanshi), magmatic polymetallic sulphide (Voisey's Bay), and unconformity-related uranium (McArthur River) deposits are also presented. Together these examples demonstrate the value that natural field EM geophysics can bring to the exploration decision making process when interpreted in context of mineral systems.

INTRODUCTION

In parallel with a general deepening of the exploration search-space over the past decade have come advances in geophysical hardware, processing, and inversion software. Besides the magnetic and gravity methods, with their inherent weaknesses being potential fields, the only other geophysical tools capable of imaging to depths on the order of kilometres are seismics, both active and passive, and natural field electromagnetic (EM) methods. Seismic reflection has seen use in mineral exploration, but the cost of mobilizing crews to remote environments *vis-à-vis* the probability of success is still considered too great for many exploration budgets. Instead, many companies are beginning to utilize less-costly passive seismic methods to image the deep mineral-systems beneath their operations, but because relatively little of this work has been published it will not be discussed further herein. That leaves natural source EM, the subject of this paper. However, the idea of using natural EM fields in mineral exploration is not new, with Morrison and Nichols (1997) having published a paper with a similar name for *Exploration '97: Geophysics and Geochemistry at the Millennium*. This paper thus can be considered a sequel, 20 years on.

For minerals, the Audio-Magnetotelluric (AMT) method is still the main approach at the deposit scale, but there is growing interest in broadband Magnetotellurics (MT) for deep crustal imaging, and long-period MT for imaging through to the upper mantle. Combined, these methods provide information across multiple scales, down to sub-continental lithospheric architecture. Although AMT and MT surveys were once clearly distinguished by different sets of equipment, with MT also often viewed as purely an academic pursuit, this distinction is now blurred by readily available commercial systems using broadband induction coils commonly acquiring data from 0.0001 Hz up to 10,000 Hz. Surveys designed to exploit this broadband capability can form a more complete picture of the deep mineral system. In this paper AMT is still used for historical continuity, although it is applied interchangeably with the more general MT in accordance with the less band-limited state of modern practice.

The biggest development in the past decade is undoubtedly the rapid advancement and uptake of Geotech Ltd.'s Z-Axis Tipper Electromagnetic (ZTEM), an airborne natural field EM system.

In "Proceedings of Exploration 17: Sixth Decennial International Conference on Mineral Exploration" edited by V. Tschirhart and M.D. Thomas, 2017, p. 349–377

Geotech acquired a total of 33,706 line-km of commercial surveys prior to *Exploration '07* and surveyed over 373,000 line-km since, suggesting that ZTEM is now a mature-technology.

This paper reviews the principles of MT, Magnetovariational Soundings, and ZTEM; highlights significant advances in those methods over the past 10 years; provides specific examples from iron-oxide-copper-gold, porphyry and sedimentary copper, magmatic polymetallic sulphide, and uranium deposit types; and ends with a summary discussion and a look to the future.

THEORY

Magnetotellurics

The theory behind MT has been reviewed by many authors, and interested readers are directed to Simpson and Bahr (2005), Unsworth (2007), Chave and Jones (2012), or Jones' (2017) paper in this volume, and references therein. A brief introduction follows regardless. The name *magnetotelluric* derives from *magneto*, ascribed to magnetic fields, and *telluric* referring to electric fields in the ground (*tellus* being the Latin word for Earth). MT therefore measures both the natural electric ($\vec{\boldsymbol{E}}$) and magnetic ($\vec{\boldsymbol{H}}$) components of EM waves to image the earth's electrical-conductivity structure.

The method was independently discovered by Tikhonov (1950), Rikitake (1950), and Cagniard (1953), who developed equations relating the ratio of orthogonal, horizontally-polarized electric- and magnetic- fields associated with tellurics (currents) to the resistivity profile beneath the measurement. By taking the ratio, they solved the problem of not knowing the source amplitude.

Magnetotelluric signals for frequencies <1 Hz originate in the magnetosphere and are termed micropulsations, while signals >1 Hz come from distant lightning strikes and are known as sferics. Together, these allow MT surveys to acquire broadband data, thereby providing an inherent depth-imaging capability otherwise lacking in potential field methods that do not contain multiple-frequency information at each point in space. The sources of the EM signals are ideally far away, which produce near-planar waves that refract vertically downward when they impinge upon Earth's surface, such that only horizontally-polarized fields exist in a 1D (layered) Earth. The resistivity (ρ) of a half-space is given by:

$$\rho = \frac{1}{2\pi f \mu_0} |\boldsymbol{Z}|^2 \qquad (1)$$

where f is frequency, μ_0 is the magnetic permeability of free space, and $\boldsymbol{Z}$ is a 2×2 tensor or transfer function known as the characteristic impedance, itself derived from $\vec{\boldsymbol{E}} = \boldsymbol{Z}\vec{\boldsymbol{H}}$. Here, the term *transfer function* refers to an Earth model that describes a linear system with an input and a predictable output (Simpson and Bahr, 2005). For non-half-spaces (*i.e.* 1D = layered, 2D = infinite strike, or 3D), $\boldsymbol{Z}$ becomes a generalised, frequency-dependent tensor:

$$\begin{bmatrix} E_x(f) \\ E_y(f) \end{bmatrix} = \begin{bmatrix} Z_{xx}(f) & Z_{xy}(f) \\ Z_{yx}(f) & Z_{yy}(f) \end{bmatrix} \begin{bmatrix} H_x(f) \\ H_y(f) \end{bmatrix} \qquad (2)$$

from which can be calculated an apparent resistivity that represents the bulk resistivity of the volume sampled by the polarized current flow as measured by the associated impedance tensor component ($\boldsymbol{Z}_{xy}$):

$$\rho_{xy} = \frac{1}{2\pi f \mu_0} |\boldsymbol{Z}_{xy}|^2 \qquad (3)$$

A corresponding phase is also defined as:

$$\varphi_{xy} = \tan^{-1}\left(\frac{Im(\boldsymbol{Z}_{xy})}{Re(\boldsymbol{Z}_{xy})}\right) \qquad (4)$$

where Re and Im denote the real and imaginary parts of $\boldsymbol{Z}_{xy}$. Intuitively, phase can be thought of a leading indicator to the apparent resistivity curve: phase less than 45° indicates apparent resistivity is increasing with depth (towards lower frequencies), while phase greater than 45° indicates it is decreasing with depth.

Magnetotelluric waves diffuse downward with a characteristic attenuation called skin depth (δ), which relates a given frequency and resistivity to a length scale (or depth) over which the strength of the wave decays to 1/e (~36%) of its initial amplitude:

$$\delta \approx 500\sqrt{\rho/f} \qquad (5)$$

Skin depth explains the greater depth-of-investigation that can be achieved with natural field EM methods as compared to active-source EM methods. For a half-space of resistivity 50 Ωm, this would suggest a depth-of-investigation of ~650 m for a survey with a minimum frequency of 30 Hz, or ~35 km for a survey acquiring down to 0.01 Hz. The skin depth concept is also important at the high frequency end in resistive areas, where it is favourable to acquire high frequency data to skin depths less than the target depth in order to provide inversion codes with the data needed for accurate depth imaging.

The use of a time-synchronised remote-reference station to improve noise rejection in MT data dates back to Gamble et al. (1979). The basic premise behind remote referencing is that events recorded simultaneously at both the remote and roving MT sites are probably real signal while events that do not cross-correlate are probably noise. The realistic implementation of remote reference robust processing is an extremely sophisticated form of advanced statistical signal processing and there are several good options to choose from (e.g. Larsen, 1996; Egbert, 1997; Chave, 2004). Chave and Jones (2012) suggest always using a remote reference station because any noise contained in the auto-power terms for self-referenced sites will produce biased impedance estimates that typically lower the calculated apparent resistivity.

A perennial bane to those who interpret MT data is near-surface galvanic distortion. Galvanic distortions are caused by the buildup of electric charge on conductivity gradients at the boundaries of near-surface heterogeneities that are below the spatial resolution of the MT survey (Chave and Jones, 2012). They change the amplitude of the measured electric field, shifting the apparent resistivity curves equally at all frequencies

in a concept known as "static shift" (Jones, 1988). Galvanic distortions can make a 1D or 2D impedance tensors appear 3D (Groom and Bailey, 1989) and for 3D impedance tensors can cause complex mixing of differently polarized data, affecting both apparent resistivities and phases of all elements (Jones, 2011).

Individual MT measurements have traditionally been classified according to their 1D, 2D, or 3D dimensionality by calculating the Swift skew or by analyzing polar diagrams of the impedance tensor. Dimensionality analysis has historically been very important because until recently modelling was only practical for 1D and 2D data; 3D data often being modelled using 1D or 2D approaches because that was all that was possible. Unfortunately, skew, polar diagrams, and all other forms of dimensionality analysis that directly utilize impedances are susceptible to galvanic distortions. Considering that phases are unaffected by galvanic distortions for 1D and 2D (but not 3D) data, phase-tensor analysis (Caldwell et al., 2004) is now becoming a standard technique to assess dimensionality, with the added utility that it identifies the geoelectric strike direction for 2D data, thus defining the optimal data rotation for 2D modelling.

Regardless of advances in 3D inversion capabilities, dimensionality will always have an important role to play in understanding MT responses. It is still the case, and will likely remain so, that data with 1D characteristics are analyzed most effectively with 1D codes and data with 2D characteristics are analyzed most effectively with 2D codes. In the 2D situation the measured data can be decomposed into Transverse Magnetic (TM) and Transverse Electric (TE) modes (Unsworth, 2007), transverse meaning "perpendicular to the profile," given the profile is perpendicular to geoelectric strike. Perhaps less confusingly, TE and TM are now commonly referred to as E- and B-polarization respectively.

No such simplifying assumptions can be made in 3D because the structure of Earth is complicated and a consistent strike direction at all scales is not defined. The impedance tensor elements all have different magnitudes and Maxwell's equations cannot be decoupled into two orthogonal polarizations.

E-polarization is sensitive to thin strike-extensive conductors (e.g. graphitic faults) and varies smoothly across geological boundaries, while B-polarization has moderate sensitivity to thin strike-extensive resistors (e.g. dykes) that block current flow across them and exhibits extreme sensitivity to geological contacts because of the buildup of charges on the boundaries. This ability to resolve geological contacts is both a blessing and a curse for MT. High resolution is obviously desirable but too high resolution can be problematic when heterogeneous overburden affects a sparsely sampled MT survey to create an aliased dataset that complicates the imaging of deeper features. This was a major motivation in the development of the continuous E-field profiling method coined Electromagnetic Array Profiling or EMAP (Bostick, 1986; Morrison and Nichols, 1997).

Magnetovariational Soundings - Tippers

Conductivity imaging is significantly augmented by acquiring the vertical magnetic-field component (H_z) in addition to the four horizontal EM-field components (E_x, E_y, H_x, H_y) related by the MT transfer-function $\boldsymbol{Z}$. The link between the horizontal and vertical components of the magnetic field is given by the vertical-magnetic transfer-function $\boldsymbol{T}$:

$$H_z = \boldsymbol{T}\vec{\boldsymbol{H}} = (T_{zx} \quad T_{zy}) \begin{pmatrix} H_x \\ H_y \end{pmatrix} \tag{6}$$

In the academic community, ground surveys that make use of vertical-magnetic transfer-functions are known as Magnetovariational Soundings (MVS) or Geomagnetic Depth Soundings (GDS). T_{zx} and T_{zy} data are commonly known as tippers because they "tip" the magnetic field from being purely horizontal to having a non-zero vertical component in response to 3D conductivity variations or to 2D E-polarization. For 2D B-polarization or in 1D geology for a plane-wave source, no vertical magnetic field is generated and the tippers are zero.

By Ampère's Law, current flow along geological strike in the *x*-direction (perpendicular to the profile) will produce magnetic fields circulating in the *y*-*z* plane, yielding a positive T_{zy} value on one side of the conductor and a negative T_{zy} value on the opposite side. This characteristic cross-over, similar to a controlled-source remote transmitter Very-Low Frequency (VLF) response, yields a powerful capability to infer the presence of a conductor between two widely-spaced tipper sites. However, tipper responses are considerably diminished for compact 3D bodies where the build-up of charge on the contacts ensures continuity of current across boundaries (Wannamaker et al., 1984).

A major benefit of tipper data being *magnetovariational* (H-field only) is they are unaffected by the galvanic distortions that complicate *telluric* (E-field) data, which in turn affect the MT impedance tensor. Moreover, unlike for E-field sensors, there is no requirement for magnetic sensors to directly contact the ground. Perhaps the most interesting characteristic of tipper data is that because $H_z = 0$ in 1D geology for a plane-wave source, they can be uniquely sensitive to basement targets where MT data are swamped by a conductive-layering response.

In contrast to MT impedance data, tippers are dimensionless ratios of magnetic fields, which leaves them in an awkward spot: sensitive to current density variations caused by conductivity contrasts, but not to the absolute conductivities themselves. However, a survey that combines both MT and tipper transfer-functions forms a more complete picture where the strengths of each data type compensates for the weaknesses of the other, thus enabling superior imaging.

ZTEM

ZTEM is a particular type of magnetovariational (tipper) survey where the vertical magnetic field is measured from an airborne platform (most commonly a helicopter) with a towed loop and the horizontal magnetic fields are measured at a fixed ground-reference station.

First flown in 2006 (Lo et al., 2009) and briefly mentioned at *Exploration '07* (Thomson et al., 2007), ZTEM is a modern variant of the Audio Frequency Magnetic (AFMAG) method initially proposed by Ward (1959, 1960). In Ward's initial AFMAG variant, the tilt-component of the magnetic field was measured only along the flight direction, which proved to be limiting. Key to the evolution of AFMAG was a paper published by Vozoff (1972) that demonstrated that the tipper needed to be computed with respect to both components of the horizontal field.

However, despite the theoretical understanding at the time, designing a system with analog components proved impractical and the AFMAG idea remained dormant for another 15 years, until Geotech Ltd. revisited it in 2000 using digital technology and modern digital-signal processing tools (Kuzmin et al., 2005). Commercial ZTEM surveys began in 2006, and while the system has continued to evolve, the best descriptions of the systems are provided in some earlier publications, namely Kuzmin et al. (2005) and Lo et al. (2006).

For ZTEM, Equation 6 is re-written to take into account that the horizontal component magnetic fields (H_x and H_y) are always being measured at a stationary base station position (r_0) while the vertical component magnetic field is measured from the mobile airborne platform (r):

$$H_z(r) = T_{zx}(r, r_0)H_x(r_0) + T_{zy}(r, r_0)H_y(r_0) \qquad (7)$$

T_{zx} and T_{zy} are two unknowns in one equation, so solving for them requires measuring the magnetic fields for at least two independent signal event polarisations, as denoted with superscripts (1) and (2) below (Holtham and Oldenburg, 2010):

$$T_{zx} = \frac{H_y^{(2)}H_z^{(1)} - H_y^{(1)}H_z^{(2)}}{H_x^{(1)}H_y^{(2)} - H_x^{(2)}H_y^{(1)}} \qquad (8a)$$

and

$$T_{zy} = \frac{-H_x^{(2)}H_z^{(1)} + H_x^{(1)}H_z^{(2)}}{H_x^{(1)}H_y^{(2)} - H_x^{(2)}H_y^{(1)}} \qquad (8b)$$

In practice, to reduce the effects of noise, multiple signal events from sliding time-series windows are combined to estimate each $[T_{zx}, T_{zy}]$ pair by minimising the least-squared error.

Equations 7 and 8 explain the major breakthrough for ZTEM as compared to previous attempts to develop an airborne AFMAG system: by measuring the horizontal fields $H_x(r_0)$ and $H_y(r_0)$ at a base station on the ground, motion noise in the airborne vertical field $H_z(r)$ data is uncorrelated and hence can be largely removed. Note that the ZTEM base station is undertaking the role of the local horizontal magnetic field reference, as would normally be employed by a pair of coils at each site for ground magnetovariational soundings. ZTEM surveys do not currently utilize a remote reference station to de-noise the data, as is standard for MT surveys. Although this would reduce the risk of noise in the base station data causing biased tipper estimates (Labson, 1985), it has not been implemented at present. Thus, ZTEM surveys are faced with a dilemma in competing requirements to place the base station close to the survey grid, to accurately represent the local H_x, H_y, and to position it far enough away that any cultural noise on the survey grid is uncorrelated.

Because the natural plane-wave source utilized by ZTEM has no (or only minimal) geometric decay, the only geometric decay it is subjected to is the fall off of the secondary-field, as opposed to an active-source system with a small dipole receiver (relative to the total distance to and the dimensions of the target) where both the primary and secondary magnetic fields fall off geometrically. For this reason, ZTEM data are much less affected by changes in terrain clearance that occur in mountainous regions where a low and consistent drape cannot practically be achieved. The lack of geometric decay in the source field also gives ZTEM the best depth-of-investigation amongst airborne EM systems in resistive areas, while in conductive regions ZTEM's depth-of-investigation is comparable to that of the more powerful airborne active-source TEM systems (Sattel and Witherly, 2012).

ZTEM has typically collected data between 30–720 Hz, depending on the signal strength measured by the airborne receiver. The low frequency limit of ZTEM is primarily related to motion-induced noise in the coil, the speed of the aircraft and the amount of data stacking. The natural EM field amplitudes are strongest at the mid frequencies measured by ZTEM, while the upper frequency of 720 Hz lies close to the AMT dead band, where between 1 5 kHz signal levels are typically reduced by one to two orders of magnitude (Chave and Jones, 2012). As such, processing and extraction of 720 Hz tipper data can be challenging. Recent upgrades to ferrite-cored base-station coils and improved time-series processing has lowered the bottom end to ~20 Hz under favourable flying conditions.

Despite its drawbacks, namely the lack of an intrinsic apparent-resistivity measurement, lack of ability to image layered geology, and a reduced bandwidth with respect to MT and ground tipper data, ZTEM offers a unique capability to collect large swaths of dense data, often in remote areas, more rapidly and at lower cost as compared to ground surveys.

THE LAST 10 YEARS

Technological developments more often follow an evolutionary path with incremental advances occurring throughout time, although from time-to-time there are step changes and the implementation of completely innovative ideas. With respect to natural field EM geophysics, the closest it has come to a true step-change in the last decade is the introduction of ZTEM, although technical development of this system began slightly more than 10 years ago and was itself seeded by ideas stemming from earlier AFMAG systems. Other innovations, like 3D inversion, clearly follow from earlier 2D work that followed upon initial 1D codes. Regardless, there have been significant improvements in our ability to collect, process, and invert natural field EM data, all leading towards better and more interpretable products.

To document the top developments since *Exploration '07* we solicited the opinions of several experts, which we combined with our own knowledge to produce the following list. Jones'

(2017) paper in this volume provides further background on these and other developments in MT.

Advances in Survey Design

Multiparameter surveys collecting conventional resistivity and chargeability data or Controlled Source Electromagetic (CSEM) data have seen incremental improvements in the last 10 years, mostly through **cheaper electronics** that has allowed for the deployment of more receivers in both 2D and 3D Distributed Array Systems, which provide the additional data modern inversion codes require (T. Ritchie, pers. comm.). The use of 2D EMAP-style surveys (Kingman et al., 2007) with their excellent along-line resolution and efficient use of equipment has also progressed with the incorporation of additional E_y dipoles and H_x and H_y coils throughout the array.

Surveys are also getting larger, with site collection increasing from tens to hundreds to thousands of stations for the largest surveys over the past decade (G. Heinson, pers. comm.). The **added data density** provides redundancy and increased spatial resolution that assists with modelling.

Advances in Data Acquisition

24-bit signal processing has greatly improved the ability to measure the electric field (Bernard Friedrichs, pers. comm.). Although the signal itself may contain only 8–10 bits of signal, the drift in the electric field and sferic spikes requires this increased fidelity to properly extract the signal from the noise. Additionally, with MT data acquisition evolving away from research and into industry, manufacturers are also beginning to construct equipment that is **simpler to operate**.

The development of **broadband coils**, from DC - 10 kHz now permits the simultaneous collection of both high-frequency AMT and low-frequency MT data in a single run for a broadband MT sounding without mode switching and without operator intervention (Killeen, 2017; Y. Avram, pers. comm.). Since measurements are typically made overnight when the signal is strongest, the amount of AMT data collected is much larger, thus minimizing the impact of the AMT dead band. Broadband data allows for better resolution of the near-surface and assists with the recognition of galvanic distortions.

Capacitive line-antennas (Hibbs et al., 2012) offer the possibility of improved measurement of the electric field by eliminating contact-resistance distortions, which are difficult to avoid, especially above 1–3 kHz (D. Goldak, pers. comm.).

Advances in Data Processing

Real-time remote-reference data monitoring (T. Ritchie, pers. comm.) allows for data Quality Control (QC) during acquisition, made possible by 3G mobile phone networks even in remote locations. In-field QC enables operators to adjust gains and replace faulty sensors, improving productivity and reducing cost. Advances in computing power also allow multiple stations to be reviewed in parallel along the lines of Egbert (1997), in real time, to rapidly identify QC issues.

With respect to computing **MT transfer functions**, Campaynà et al. (2014) proposed a new methodology called Estimation of Local transfer-functions by Combining Interstation Transfer-functions (ELICIT) whereby the MT tensor relationships of the local site are derived using only interstation transfer functions. The main property of the ELICIT method is that the employed interstation transfer functions are independently constrained, without the need to acquire the electric and the magnetic fields at two stations simultaneously to recover the local MT tensor relationships, offering new possibilities for MT data acquisition and processing when the magnetic time-series at the local site are affected by local noise or are truncated.

Advances in Data Inversion

Over the last decade, there has been a **move from 2D to 3D modelling and interpretation**, mostly in academia but more-and-more in industry. Although MT inversions are still mostly unconstrained (G. Heinson, pers. comm.), the trend to interpret the full impedance tensor is a big step forward. The use of 3D inversions is also making dimensionality arguments moot—the codes simply deal with it. But more data and larger meshes has also brought about the need for faster computers with more memory, with some organizations moving their inversions to the cloud (Theil et al., 2012).

Four principal codes were developed in the last decade: **MARE2DEM** (Key and Ovall, 2011; Key, 2012) at the University of California at San Diego, **ModEM** (Egbert and Kelbert, 2012; Kelbert et al., 2014) at Oregon State University, **EMVision-MT3D** (Gribenko and Zhdanov, 2015) from the University of Utah, and **MTZ3D** (Holtham and Oldenburg, 2010) at the University of British Columbia (UBC).

MARE2DEM is a freely available, open source, adaptive 2D forward and inverse finite-element code for EM geophysics. Originally designed with marine-CSEM and -MT applications in mind, it can also be applied to onshore EM modelling problems using both active and passive sources simultaneously. A distinguishing feature of this code is that rather than using rectangular voxels defined in advance by the user, it generates an unstructured finite element mesh that is adaptively refined automatically as required according to the complexity of the model. A key benefit of the tessellated mesh is that topographic slopes can be modelled continuously, rather than being broken up into discrete blocks at the pre-ordained resolution of a regular grid. For many marine environments and petroleum exploration scenarios the 2D approximation is sufficient to model the data very accurately. However, this is less often the case for mineral exploration where ore systems are more discrete and topography can be highly variable in both the in-line and cross-line directions.

ModEM (Modular EM) is a 3D MT inversion program based on object-oriented design principles that allow for different inversion algorithms to be seamlessly interchanged and for new capabilities to be rapidly implemented. Publications citing ModEM for regional- and continental-scale 3D inversions include Piña-Varas and Dentith (2016) and Thiel et al. (2016) for surveys in Australia and Meqbel et al. (2014) in the USA. Freeware for non-commercial use, ModEM is largely

supplanting the use of 2D inversion codes. Perhaps most importantly, by making a usable and effective 3D MT inversion code available in academia, ModEM is training the next generation of users familiar with 3D EM inversion methods, who will ultimately contribute to the ongoing use of 3D EM inversion in exploration.

An integral equation code, EMVision-MT3D includes a data-space formulation with variable-sensitivity domains and distortion correction for efficient implementation at different scales. Input data types include: standard MT impedances with or without tippers, ZTEM data, and controlled-source data from grounded wires or loops. The code has been successfully applied to a number of mining and geothermal exploration data sets, as well as continental-scale lithosphere studies (e.g. Paré et al., 2012; Zhdanov et al., 2011; and Zhdanov et al., 2012).

MTZ3D is the commercial version of UBC's MT+ZTEM inversion software, which uses standard rectilinear cells (Holtham and Oldenburg, 2010). Additionally, sponsors of the UBC Industrial Research Chair (IRC) in Computational Geophysics have access to E3DMT that uses an OcTree mesh to discretize the earth (Haber et al., 2012). Although still rectilinear, the OcTree implementation allows for changes in both the horizontal and vertical cell dimensions throughout the voxel mesh to accommodate for high spatial gradients. Small cells near-surface better account for statics and accommodate rough topography while large cells at depth correspond to the lower frequencies that sample them, thereby reducing computational overhead.

The past 10 years has also witnessed a burgeoning number of companies offering 3D inversion services for ZTEM data. Computational Geosciences Inc., Condor Consulting Inc., Mira Geoscience Ltd., and Geotech Ltd. all use the UBC codes, while ModEM and TechnoImaging use their own proprietary software.

A final major development of late, whose significance will continue to unfold over the next 10 years, is the advent of **joint inversion** techniques that combine airborne ZTEM data with ground MT sites, the latter of which provide the critical electric field information to produce robust 3D conductivity images to kilometres depths. This is discussed in detail in a subsequent section.

Advances in Handling Galvanic Distortion

Galvanic distortion has traditionally been addressed by acquiring other data at the measurement site to provide an independent estimate of the near-surface resistivity, such as from an IP/resistivity survey or a TEM sounding. These other methods indicate where problems may exist and the interpreter must then decide how to handle them. Modern 3D inversions provide another option: model them. This can be accomplished by increasing the resolution of the MT experiment by measuring higher frequencies and then increasing the resolution of the mesh in the near-surface and near the electrodes. Regardless, no substitute exists for an experienced interpreter who understands how to recognize and address distortions.

Advances in Related Fields

Although not a natural field method, the use of CSEM, especially by the petroleum industry in the marine environment has produced numerous advances in signal process and in inversion methods, such as the freeware Occam 1D inversion code (Constable et al., 1986). CSEM is itself a modern variant of the Controlled Source AMT (CSAMT) method popularized in the 1980s and 1990s by Zonge Engineering, amongst others (Zonge and Hughes, 1991).

Advances in ZTEM Interpretation

The first ZTEM survey-deliverables included up to 24 channels of data and an equal number of grids, namely the in-phase (real) and quadrature (imaginary) parts (2) for each frequency (usually 6, spanning roughly 30–720 Hz) for both the in-line (T_{zx}) and cross-line (T_{zy}) orthogonal components (2). This proved to be intractable because tipper responses bear little resemblance to the known geology. Note that for ZTEM, T_{zx} refers to the in-line tipper, whereas for MT it can be either T_{zx} or T_{zy}, depending on whether x or y is the line direction.

Advanced map-based products were devised at various times in attempts to improve both the quality and utility of the deliverables. These "filters" all had the common objective of transforming cross-over style tipper responses into peaks, and as such they are analogous to the Fraser filter (Fraser, 1969). The output was a plan-view image, not dissimilar to the Reduction to Pole (RTP) filter that places peaks on top of magnetic sources.

The first advanced-interpretation product employed was the 90-degree Phase Rotation (PR) filter, which converts along-line and across-line cross-over anomalies into peaks. The challenge with PR was that it could only look at one component at a time, so the subsequent inclusion of both T_{zx} and T_{zy} components into a single "resultant phase" or Total Phase Rotation (TPR) map-product (see Lo et al., 2009) was a worthy advancement in interpretation, often producing reasonable-looking, if broad, positive and negative anomalies for both components/directions combined (J. Legault, pers. comm.).

Following the TPR filter, the next step towards more robust interpretation was the Total Divergence (DT) filter. The rotationally-invariant DT (Kuzmin et al., 2005), which itself is analogous to the Peaker parameter of Pedersen (1998), sums the horizontal derivatives $\partial T_{zx}/\partial x$ and $\partial T_{zy}/\partial y$ to obtain peak responses over conductors (Legault et al., 2009), but unfortunately also over topographic highs (especially in the higher frequencies). The nature of the derivative function helped highlight shallow, discrete linear-targets and regional lineaments; however, long wavelength, low amplitude deeper targets are generally too noisy to produce coherent DT responses. Ultimately this susceptibility to noise limited the usefulness of the DT filter.

Beginning in 2008, another attempt to display the survey results in plan view used the Karous-Hjelt (KH) filter (Karous and Hjelt, 1983) in 2008. However, like the PR, KH filters could only be applied to single-component directions (x or y) and to single frequencies at a time, thus resulting in a similarly

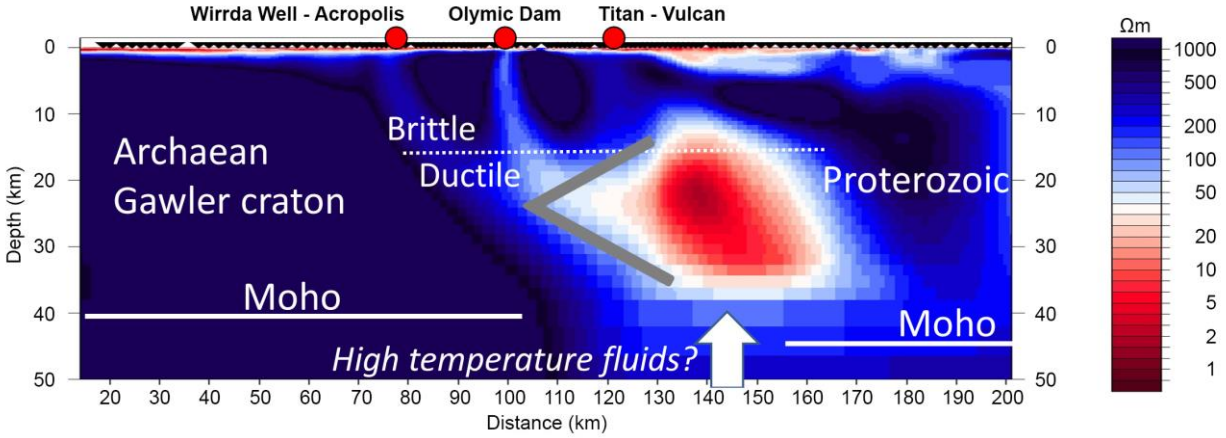

Figure 1: Regional MT transect 2D inversion over Olympic Dam (modified from Heinson et al., 2016).

substantial number of map products. Later, Sattel et al. (2010) introduced the apparent conductivity (AppCon) transform of Becken and Pedersen (2003) from VLF–EM, with the intent of combining both the T_{zx} and T_{zy} components into a single map for each frequency.

The advantage of the TPR, DT, and AppCon filters was to reduce the number of map products from two to one per frequency. However, a common failing amongst them was that they only extracted information from the in-phase (real) component. Prior to the introduction of inversion in 2008, interpretations were focussed on in-phase cross-overs because of the non-intuitive relationships between the in-phase and out-of-phase (quadrature) amplitudes versus frequency, as well as the confusing relationship of sign flips, with the quadrature component often being opposite in sign to the in-phase. As a result, the quadrature maps were largely ignored or omitted entirely. Perhaps the most significant failing of all the grid filters is their inability to deal with rugged topography.

Therefore, the greatest advancement in ZTEM interpretation was certainly inversion-modelling, with oddly enough, 3D coming before 2D inversion. Indeed, from the outset, ZTEM tipper behaviour had been studied and predicted with 3D forward modelling using Petros Eikon Incorporated's EMigma code (based on the method of Habashy et al., 1993) and the UBC MT3D code (see Lo and Zang, 2008). However, the inspiration for 2D inversion was Persson et al.'s (2008) presentation on the inversion of VLF data at AEM2008 as well as Holtham and Oldenburg's (2008) presentation of the ongoing work at UBC at the SEG meeting later that year. Both the 2D and 3D codes utilized were able to account for topography along the flight lines.

As UBC's MTZ3D inversion code was only available to consortium sponsors in 2008, Geotech contracted Phil Wannamaker to provide a 2D code that he based on de Lugao and Wannamaker (1996), as described in Legault et al. (2009). By 2009, their code was being used to invert all ZTEM survey data. Sattel and Witherly (2010) would later introduce an adapted version of the Occam 2D code of deGroot-Hedlin and Constable (1990). Being 2D, these codes only used component the in-line (T_{zx}) but still they proved to be the first instance of combining both the in-phase and quadrature components of all six frequencies into a single result. 3D inversions able to include both T_{zx} and T_{zy} remained in the domain of academics and their major-company sponsors until 2012 when the non-OcTree version of MT3D became commercially available.

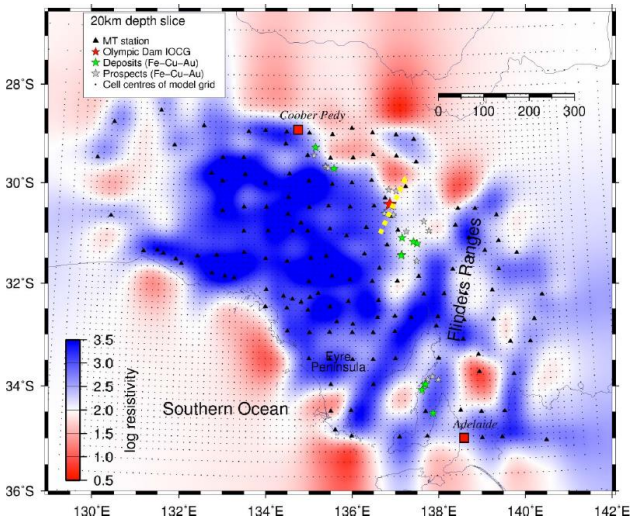

Figure 2: South Australia AusLAMP 3D MT inversion resistivity depth slice at 20 km (after Thiel et al., 2016). The yellow dots indicate the position of the regional transect over OD in Figure 1, the black dots the inversion grid notes, and the black triangles the survey sites. The model is best constrained beneath the stations.

Regardless, the trick with all ZTEM inversions is the starting model half-space resistivity. As explained earlier, ZTEM measurements are not direct proxies for resistivity like MT measurements are, and so obtaining reliable conductivity-depth distributions from either 2D or 3D ZTEM inversions is dependent on a reasonably accurate resistivity starting model. One method to determine the resistivity is to analyse profiles over topographic peaks. Both the resistivity and topography play a role in the response but the topography is known, so a

best-fit resistivity can be identified by modelling different values in an analogous manner to Nettleton's method in gravity. Otherwise, Holtham and Oldenburg (2010) showed that trial forward calculations can help determine a suitable starting model.

APPLICATIONS TO MINERAL SYSTEMS

IOCG

As stated at the outset, the exploration search-space is expanding to depth in concert with an emerging understanding of mineral systems (McCuaig and Hronsky, 2014). Heinson et al. (2006) offer a thought provoking example of using MT to illuminate deep aspects of the ore-forming system at Olympic Dam (OD). Emplaced at the margin of the Proterozoic Gawler Craton in South Australia, Olympic Dam is the world's sixth largest copper deposit and its largest uranium deposit. Low frequency (0.0001–0.1 Hz) MT sites were acquired along a regional transect across the deposit, coincident to a deep-crustal seismic reflection profile, first at 5–10 km station spacing in 2005 and then infilled to 1–2 km stations with additional sites lengthening the profile in 2014–2016 (Heinson et al., 2016).

Figure 1 presents a 2D inversion of their 200 km-long MT transect that traverses the Moho to 50 km depth and suggests the altered remnants of a fluid pathway connecting Olympic Dam to a deep mineralizing reservoir, along with secondary conduits linking to other known IOCG mineralized zones. The geoelectric section is strikingly similar to the porphyry mineral system schematic of Sillitoe (2010), shown in Figure 3, reinforcing the mineral systems concept of large-scale commonalities of ore-forming processes over disparate deposit models.

Recent results from the Australian Lithospheric Architecture Magnetotelluric Project (AusLAMP), a government-sponsored long-period MT survey aiming to cover the entire Australian continent with 55 km spaced sites, have substantiated this work and reaffirmed its significance. Depth slices through the ModEM 3D inversion of the Gawler region AusLAMP data shown in Figure 2 suggest that the craton is largely resistive but has a prominent deep conductive feature wrapping around its eastern margin. The major IOCG deposits of Prominent Hill, Olympic Dam, and Carapateena sit on the gradient of this feature while the Moonta and Hillside deposits are on similar boundaries.

The AusLAMP 3D depth slices correlate well with the higher-resolution 2D MT model of Heinson et al. (2016), together revealing both the lateral continuity of the conductive feature and its vertical extent from the upper mantle through to the brittle-ductile transition (Soeffky et al., 2015). These results support the conclusions of Griffen et al. (2013), in the context of magmatic deposits, by linking the fertile sub-continental lithospheric mantle to the upper crust through large-scale fluid pathways formed at craton margins. Moreover, they offer a tangible and compelling demonstration of the technical capability to incorporate the entire lithosphere in regional targeting using a combination of MT surveys tuned to various scales.

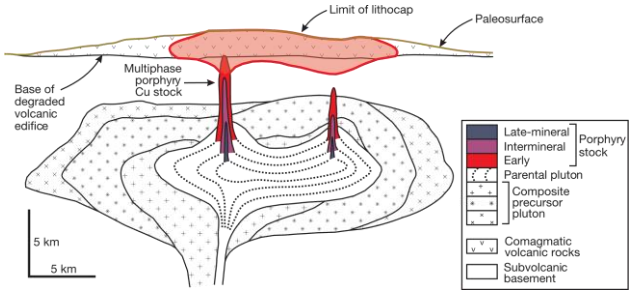

Figure 3: Generalized spatial relationships between porphyry Cu stocks, underlying pluton, overlying comagmatic volcanic rocks in a porphyry mineral system (after Sillitoe, 2010).

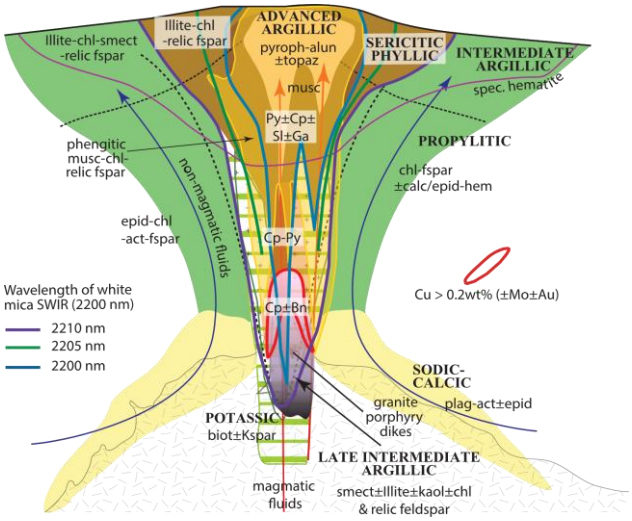

Figure 4: Generalized hydrothermal alteration model for a porphyry system footprint (after Halley et al., 2015).

Porphyry Deposits

Accounting for ~70% of the global Cu inventory (Sillitoe, 2012), porphyry deposits are also the world's largest source of Mo and are among the largest sources of gold production (Sillitoe, 2010). As described by Holliday and Cooke (2007) at *Exploration '07*, the porphyry deposit model in Figures 3 and 4 is recognized as one of the crowning achievements of economic geology, beginning with Lowell and Guilbert's (1970) seminal paper.

Induced polarization (IP) and airborne magnetics (AMAG) have historically been the most common geophysical methods applied to the exploration for porphyry-copper deposits (PCDs) (Holliday and Cooke, 2007). AMAG is ubiquitous in PCD exploration programs because of its low cost relative to its value as an aid to geological and structural mapping together with its ability to target some classes of PCDs directly (Hoschke, 2011). Similarly, IP has been used extensively for its ability to map chargeable minerals associated with the broad-scale alteration footprint of porphyry systems. The method usually responds more strongly to the outer pyrite shell than to the inner core of copper-sulphide mineralization.

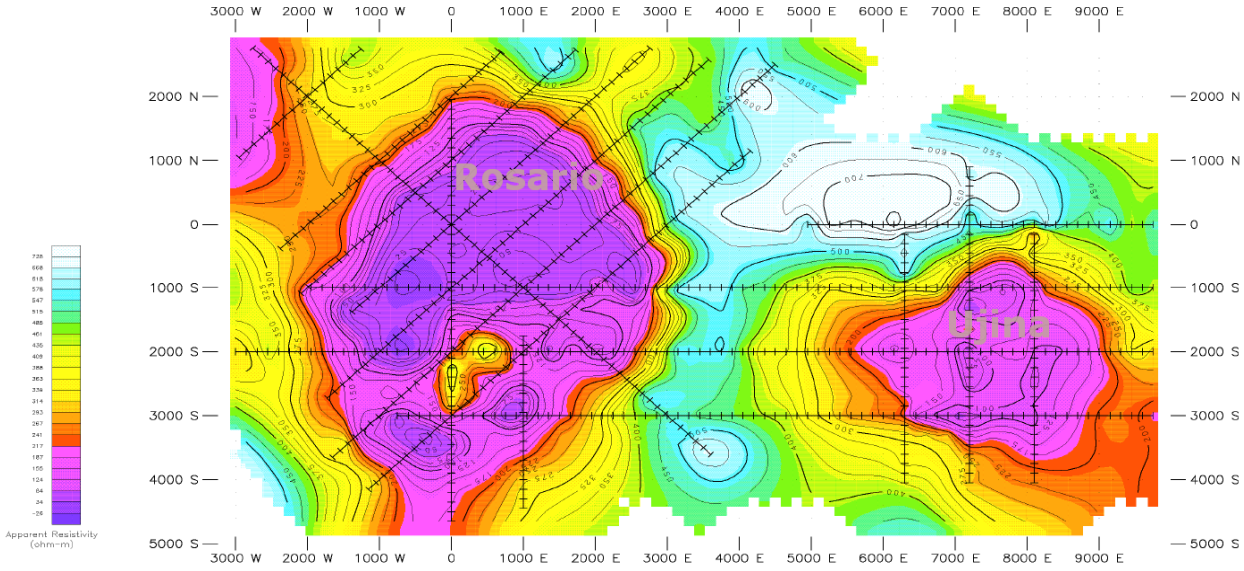

Figure 5: Plan image produced from 1990s era Collahuasi dipole-dipole DC Resistivity data (modified from Hoschke, 2001).

Collahuasi, Chile

The Ujina deposit in Chile's Collahuasi district is likely the most famous example of a major PCD directly discovered by targeting a geophysically-defined conductor. Ironically, the story is often remembered for the initial holes targeting the strongest dipole-dipole IP response, which found a halo of barren pyrite, rather than the discovery-hole targeting the DC resistivity-low that returned 62 m at >2% Cu (Watts, 2002) (see Figure 5).

Subsequent drilling at Ujina identified a 127 Mt supergene resource grading 1.8% Cu in addition to the main 0.8% Cu, 1.2 Bt hypogene deposit, establishing the merit of targeting geophysical conductors in a porphyry setting. Attention then shifted to the larger and lower resistivity zone outlined by the DC Resistivity survey in proximity to the historical Rosario vein system, termed the Collahuasi anomaly. Drilling into this conductive target lead to the discovery of an extensive network of vein-hosted to semi-massive high-grade Cu mineralization that ultimately proved to be one of the world's greatest mineral deposits. Among the top-five copper producers in operation, the Collahuasi mine is owned by Anglo American plc and Glencore plc (44% each) and a consortium of Japanese companies led by Mitsui (12%).

The high conductivity associated with the very-high grades of the stockwork and veining ore types at Collahuasi is not an isolated case. Nelson and Van Voorhis (1983) took 109 in-situ measurements at open-pit copper mines in the southwestern USA and demonstrated a consistent relation between resistivity and total sulphides abundance (Figure 6). When the sulphide distribution is truly disseminated with <3% total sulphides, resistivity is relatively high and variable, and bulk resistivity is primarily a function of porosity, saturation, and pore fluid salinity (Hoschke, 2011). But from 3 to 7% total sulphides, despite textures oft-described as disseminated, a consistent inverse relation between resistivity and weight percent total sulphides is observed due to a developed network of electrical

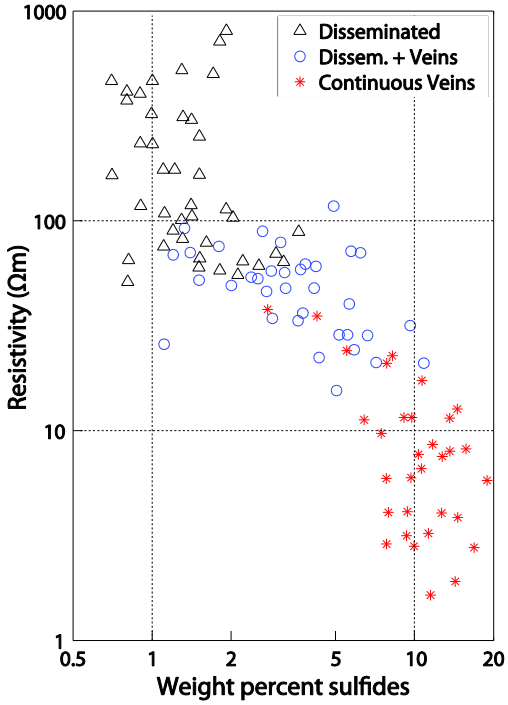

Figure 6: Relation between electrical resistivity and weight percent total sulphides based on 109 in-situ measurements by Nelson and Van Voorhis (1983) in four southwestern USA open-pit porphyry copper mines (after Lee et al., 2017).

connectivity between sulphide grains and veinlets. Resistivity drops dramatically above 7% as continuous sulphide veins form. Finally, towards 20% sulphides, bulk conductivity approaches that of massive sulphides. Nelson and Van Voorhis point out that classifying rocks within porphyry deposits based solely on their sulphide abundance neglects other resistivity-influencing parameters such as porosity, pore fluid composition, and alteration. Regardless, since brecciation and alteration intensity

are often intimately associated with sulphide abundance, it is not surprising such a consistent empirical correlation exists.

The idea to target PCDs with EM methods is not a new one. Witherly (2002) chronicled the rapid progression following the 1993 presentation of ground TEM results at Ujina that clearly imaged the high-grade supergene enrichment blanket (Dick, 1993) to an aggressive program shortly thereafter by then BHP Minerals to target the Conductive Blanket Model (CBM) with airborne TEM. Although the premise that chalcocite blankets are conductive proved to be correct, unfortunately the initiative did not result in the development of a new mine. Witherly attributed this to three factors: the difficulty for airborne EM to resolve "stacked" conductors, an under-appreciation for the number of false positives that would be generated, and an inability to gain access to prospective ground identified as hosting favourable anomalies.

Three major differences between recent uses of natural field EM for PCD targeting and the wave of enthusiasm for TEM in the 1990s are:

1. Natural field EM methods are sensitive to a broader range of conductivity contrasts, allowing more subtle variations between altered and unaltered host rock to be distinguished;

2. Natural field EM methods can achieve greater depths of investigation; and

3. With respect to airborne surveys in mountainous regions where a low and consistent terrain clearance cannot be maintained, the slower attenuation of the natural field signal compared to active source systems makes it advantageous to acquire natural field data, as previously discussed.

These characteristics shift the geophysical paradigm from one of enrichment blanket "bump hunting" to a means of imaging entire mineral systems.

Like the early oil explorers who successfully applied new developments in 3D seismic technology to their knowledge of the petroleum system, the potential of 3D imaging with natural EM fields rests in the ability of modern explorers to apply their understanding of mineral systems in the context of subsurface conductivity expressions. The following examples provide a foundation to develop this understanding and previews its potential over the next 10 years.

Pebble, Alaska

Containing over 10 Bt of mineralized rock with an enormous alteration footprint extending for kilometres (Witherly, 2014), the Pebble calc-alkalic Cu-Au-Mo porphyry deposit ranks among the world's largest Au and Cu deposits. It is comprised of two coeval 89.5–90.4 Ma hydrothermal mineralizing centres, with the shallower West zone discovered in 1989 followed by the East zone in 2005. The West zone extends from surface to approximately 500 m depth and is itself centred on four small granodiorite plugs, while the higher grade but deeper East zone, down-dropped 600–900m by a graben structure, occurs within a larger granodiorite pluton and associated sills that intrude the country rocks (Lang and Gregory, 2012).

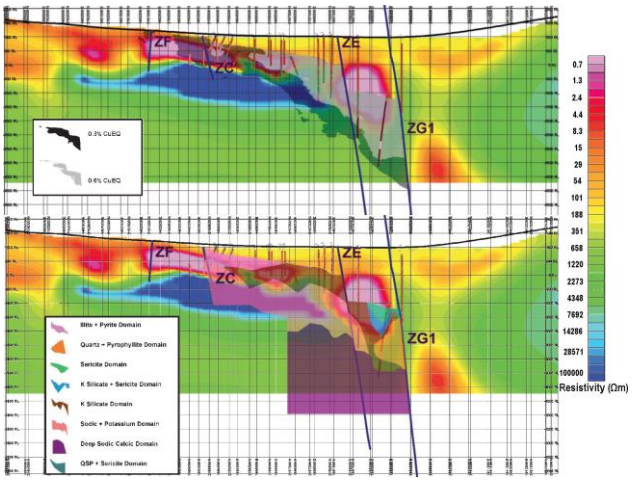

Figure 7: Pebble ZTEM 3D inversion model comparison with CuEqn mineralization shells [top] and with alteration zones [bottom] (after Paré et al., 2012, courtesy Anglo American).

A ZTEM survey acquired at 200 m line spacing across the deposit area in 2009 collected in-line (T_{zx}) and cross-line (T_{zy}) tipper data at five frequencies from 30–360 Hz. Initial interpretations utilizing the basic map images (TPR, DT, etc.) from the lower frequencies broadly outlined the extensive illite-pyrite alteration surrounding Pebble West as a zone of elevated response, while early 2D ZTEM inversion sections displayed an overall correlation with the conductive alteration system but were very limited in terms of resolution (Paré and Legault, 2010). An early application of 3D ZTEM inversion technology, in this case the method of Zhdanov et al. (2011), served to greatly improve the imaging results (Paré et al., 2012).

Figure 7 shows the correspondence between mineralization, alteration zonation, and the recovered conductivity model from the 3D ZTEM inversion. It is apparent that the highest conductivity relates to the illite-pyrite and advanced argillic parts of the system. The ore mineralization itself is, at most, a secondary influence upon the bulk conductivity at the spatial scale resolved by ZTEM. In terms of imaging the overall system, the ZTEM result would surely have drawn great attention to the potential at Pebble East and possibly accelerated its discovery had it been flown earlier. Regardless, in terms of targeting grade within a porphyry prospect, this early case study demonstrates the importance of integrating petrophysical knowledge into the exploration process.

El Salvador, Chile

Located in central Chile, the El Salvador deposit occurs in the classic structural setting of the great porphyry deposits of the Atacama, at the intersection between the arc-parallel Domeyko fault system and a transverse lineament (Sillitoe, 2010). The essential elements of the genetic model for El Salvador, as developed by Gustafson and Hunt (1975), are variations on a common theme for deposits of the central Andean middle

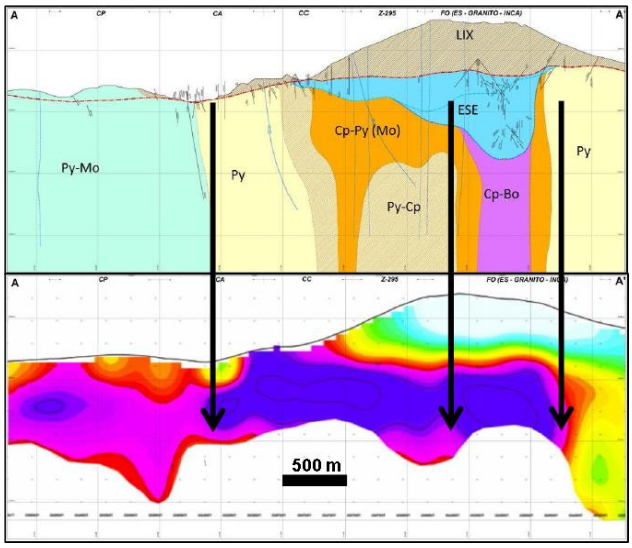

Figure 8: Sections correlating the ZTEM data inversion recovered resistivity (hot colours are lower resistivity) with different mineralized zones within the El Salvador deposit, Chile (after Cifuentes, 2014, courtesy CODELCO).

Eocene to early Oligocene porphyry Cu belt, and among porphyry systems in general.

A 2D inversion presented at the inaugural Chile Explore Congress in 2014 (Figure 8) illustrates a prominent low-resistivity zone associated with various sulphide assemblages within El Salvador, which is consistently imaged at variable depth beneath mountainous topography. An important observation is that no correlation between sulphide species and relative resistivity is apparent. It can only be said that resistivity is generally lower towards the core of the deposit than towards its fringes. The intrinsic resistivity of the various sulphide species is likely playing an insignificant role in controlling the overall resistivity variations within the deposit as compared to the major influence of total-sulphide abundance.

Los Bronces, Chile

The Late Miocene to Early Pliocene magmatic arc of central Chile ranks as the world's largest Cu district by contained metal and includes the Río Blanco-Los Bronces porphyry Cu-Mo district, endowed with >200 Mt copper (Toro et al., 2012). Deposits currently being mined in the district include Río Blanco and La Americana, operated by CODELCO, and Los Bronces, operated by Anglo American Sur S.A. More recent discoveries by Anglo American in the district at San Enrique-Monolito and at Los Sulfatos contribute over 65 Mt Cu to the inventory (Toro et al., 2012). Making these deposits unique among Chilean porphyries is the extent to which mineralization is associated with hydrothermal breccias that developed in association with porphyry phases.

In 2014, both Anglo American and CODELCO acquired ZTEM data spanning the corridor from La Paloma–Los Sulfatos to Río Blanco–Los Bronces. Initial results over the Los Bronces tenements were encouraging, although complicated by a high degree of cultural noise associated with power lines and mine infrastructure. The initial 3D inversion model was computed using the 2011 UBC MTZ3D code on a standard rectangular mesh with coarse topography. This model identified the known major features of interest but suffered from the previously mentioned complications.

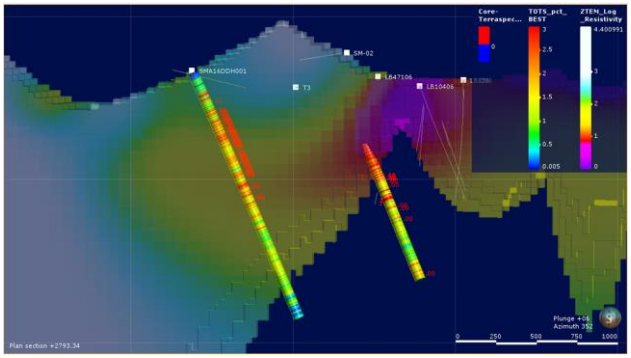

Figure 9: An example correlating total sulphur in exploration drill holes near the Los Bronces pit with a 3D ZTEM inversion resistivity model computed in-house by Anglo American. The resistivity model is cut to a realistic depth of investigation based on the integrated conductivity of the overlying cells.

Following an initiative to invigorate exploration in the Los Bronces district in 2015, the ZTEM data were re-examined with a focus on reducing the impact of cultural noise and topography. The 2016 version of the UBC E3DMT code, proprietary to IRC sponsors, was run on Anglo American's in-house computing cluster using a new technique developed to mitigate cultural noise and OcTree meshing capability to finely discretize topography based on a high-accuracy DTM.

Substantially improved conductivity-image results were obtained that have since proved to be a core component of an integrated district-scale targeting program. Figure 9 illustrates the typical imaging quality from an area near the Los Bronces open-pit. More recent work following re-processing the raw time-series by Geotech with better designed notch filters has offered further improvements.

Cobre Panama, Panama

Cobre Panama comprises a cluster of six porphyry deposits being developed as a multi-pit operation by Minera Panamá S.A. (MPSA), in which First Quantum Minerals Limited (FQML) holds an 80% equity interest. Measured and indicated resources total approximately 4.2 Bt at 0.35% Cu with additional Au, Ag, and Mo credits (FQML, 2017). The 28 Ma porphyries forming the deposits intrude andesite volcanics at the southern margin of a large Oligocene batholith. A tropical saprolite profile up to 30 m thick covers much of the area, only allowing rare outcrop glimpses through incised drainage valleys (Legault et al., 2016a).

Modern exploration at Cobre Panama was initiated by a UN program in the 1960s that used mapping, stream sediment geochemistry, and drilling to discover the Botija, Colina and Valle Grande deposits. Further work by the Adrian/Inmet/Teck consortium in the 1990s, at the then-named Petaquilla, utilized airborne magnetics to reveal the association between the known

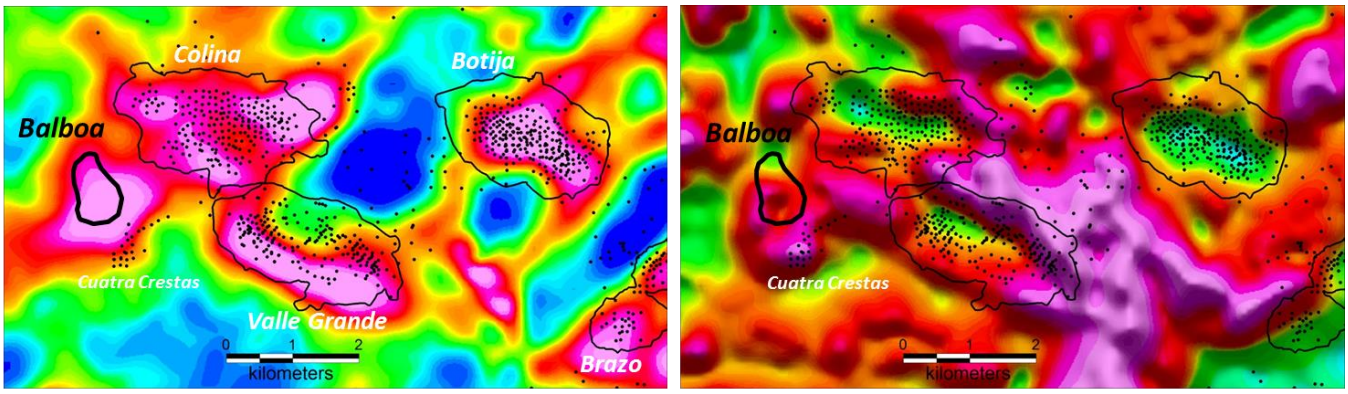

Figure 10: ZTEM survey results over the Cobre Panama deposits area; in-phase total divergence 360 Hz image with hot colours corresponding to greater ZTEM response [left], RTP mag with hot colours corresponding to higher mag response [right]. Drill hole collars shown are prior to the Balboa discovery (after Legault et al., 2016a).

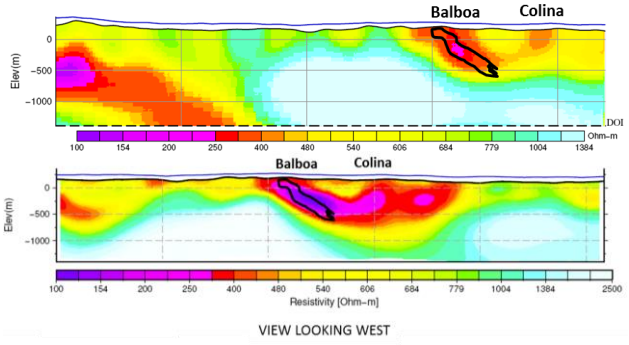

Figure 11: ZTEM 2D inversion (after Legault et al., 2016a) [above] and 3D inversion (after Legault et al., 2016b) [below] across the Balboa–Colina deposits. Note the offset between the two profiles.

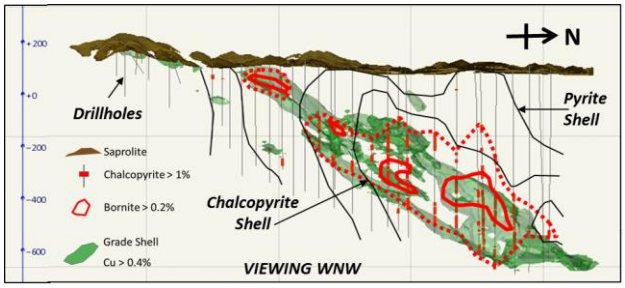

Figure 12: Balboa deposit sulphide shells (after Burge, 2014).

deposits and RTP magnetic lows, possibly related to magnetite-destructive phyllic alteration of the variably magnetized andesites. Integrating the AMAG with soil geochemistry proved to be an effective targeting strategy that resulted in discovery of the Botija West starter pit in addition to further upside at Valle Grande and Brazo–Botija Abajo (Burge, 2014).

MPSA acquired ZTEM data in 2010 with the objective of rapidly screening difficult terrain for higher-grade targets. Initial results examining the in-phase TPR images suggested a correlation with mapped near-surface sulphides and/or sericitic alteration at the higher frequencies and with the known deep sulphides of Botija in the lower frequencies. A large ZTEM anomaly northwest of the Cuatra Crestas prospect (Figure 10) was also detected in an area that had evaded previous drilling because of a thick leached-cap that rendered soil geochemistry less effective and an RTP mag response that appeared inconsistent with the signature of the other deposits (Burge, 2014), although subsequent higher-resolution AMAG did identify an RTP low at the centre of what would become the Balboa pit outline, just like the other deposits (C. Wijns, pers. comm.).

The first hole targeting a ZTEM anomaly returned 209 m at 0.28% Cu plus a deeper intersection with 2.9% Cu and 2.0 g/t Au in sheeted quartz-chalcopyrite-bornite veins over 6.4 m. The second drill hole then intersected 240 m at 0.60% Cu and 0.21 g/t Au, including 114 m at 0.92% Cu and 0.42 g/t Au, to confirm discovery of the Balboa deposit (Burge, 2014). A resource drilling program over the next 18 months proved the significance of the Balboa discovery by increasing Cobre Panama's indicated and inferred Cu and Au resources by 19% and 29% respectively (Legault et al., 2016b). Figures 11 and 12 illustrate the correspondence between the low recovered resistivity of the Balboa deposit in the ZTEM inversion sections and the drill defined sulphide shells.

Resolution, Arizona

With a resource of over 1.6 Bt at 1.47% Cu and 0.037% Mo (Hehnke et al., 2012), Resolution is truly a world class deposit. Located within the historical Superior mining district less than 100 km east of Phoenix, Arizona, being buried beneath ~1 km of post-mineral cover meant that this giant ore deposit evaded detection despite an 86-year period of nearby mining. Figure 13 shows the surface projection of Resolution's 1% Cu shell with respect to the locations of the historical mining operations in its immediate vicinity, beginning with the Silver Queen mine in 1875, later reopened as the Magma mine in 1910. The Resolution discovery-holes were drilled in 1998 based on a progression of geological reasoning that began with deep targets first postulated by Magma geologists in the 1960s (Hehnke et al., 2012).

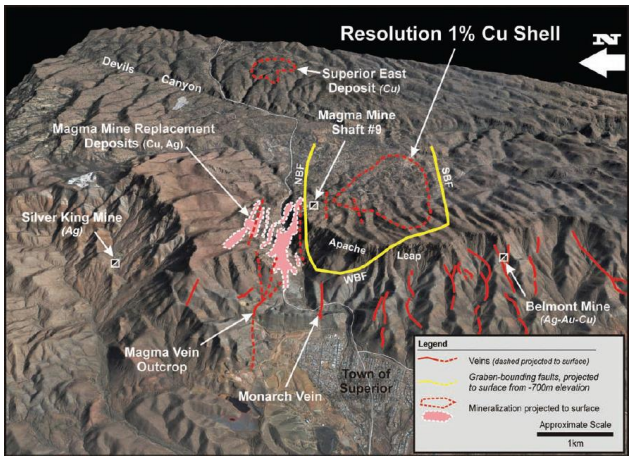

Figure 13: Aerial view showing the surface projection of the deep Resolution deposit 1% Cu shell with respect to the locations of the historical mining operations in its immediate vicinity (after Hehnke et al., 2012).

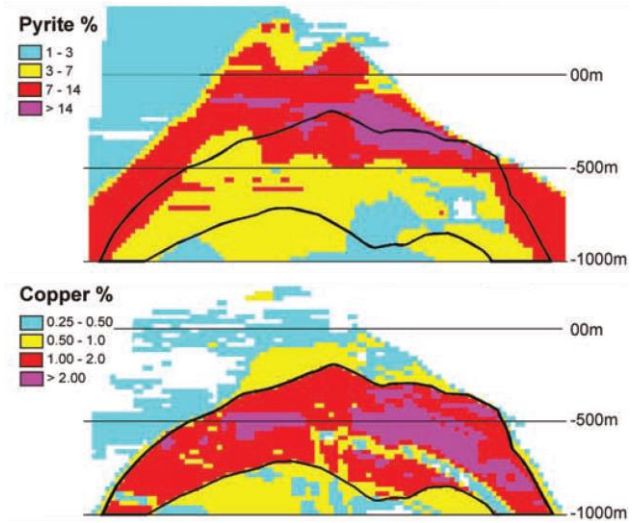

Figure 14: Resolution copper and pyrite block model shells (after Hehnke et al., 2012).

Resolution is hosted by a sequence of Proterozoic and Paleozoic clastic and carbonate sedimentary rocks and diabase sills. A swarm of Late Cretaceous quartz porphyry dikes intrudes this reactive host to produce a very high grade inner shell of chalcopyrite-dominated Cu mineralization, which is itself surrounded by an intensely pyritic outer shell that in some locales exceeds 14% by weight (Figure 14). The alteration system is concealed by at least 1 km of post-mineral cover comprised of the Tertiary Whitetail conglomerate and Apache Leap tuff that unconformably overly the Mesozoic basement (Hehnke et al., 2012).

Figure 15 shows an unconstrained 2D inversion of MT data across Resolution, first presented by McMonnies and Gerrie (2007) at *Exploration '07*. The survey's specifications are unknown, but from Equation 5 it can be inferred that a minimum frequency of about 1 Hz would be required to achieve the

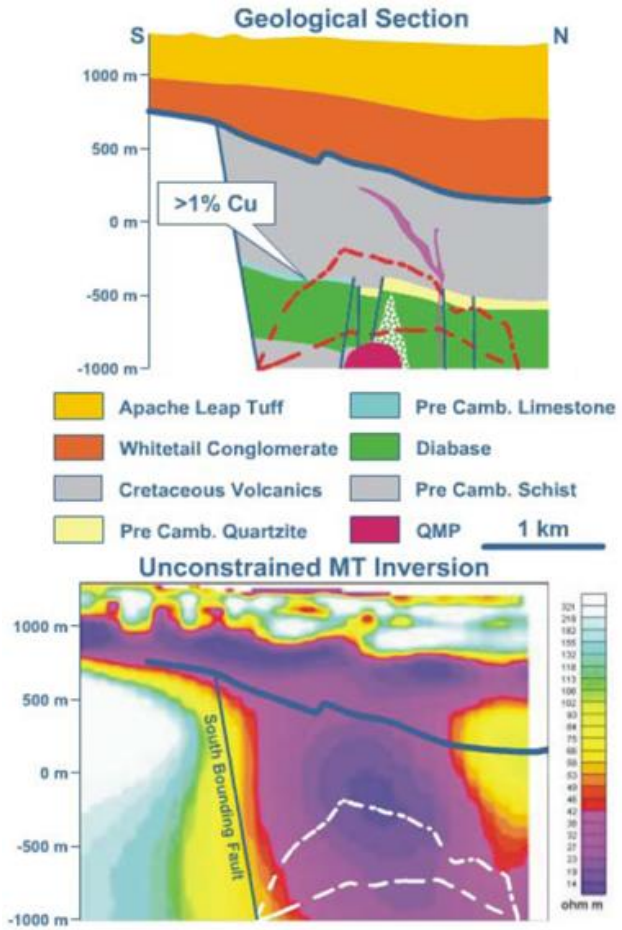

Figure 15: Resolution simplified geological section and unconstrained 2D MT inversion section (McMonnies and Gerrie, 2007).

presented depth of investigation through the conductive Whitetail conglomerate and well into the conductive deposit. The intensely-altered pyritic shell overlying the Resolution copper sulphides, in accordance with Nelson and Van Voorhis (1983), is likely to be the major source of the deep conductive response in the MT data. Given the MT method's decreasing ability to resolve features with depth and that the sensitivity to a deep target is reduced by the presence of an overlying conductive layer, the indistinct portrayal of Resolution as a seemingly continuous conductive-tube spanning from the base of the overlying conductive layer to beyond 1000 m below sea level is not surprising. However, despite the underwhelming imaging quality of this section, it suffices to say that giant conductive tubes beneath historical mining areas with well-reasoned geological potential to host superior grades at depth are justifiably attractive drill targets.

Freeport Exploration carried out a ZTEM survey across the Superior district in 2013, which covered the Resolution deposit (Witherly et al., 2016). Much of the data were deemed unusable because of excessive power line interference; fortunately however, enough data over Resolution and its immediate surrounds were of sufficient quality to carry out a 3D inversion.

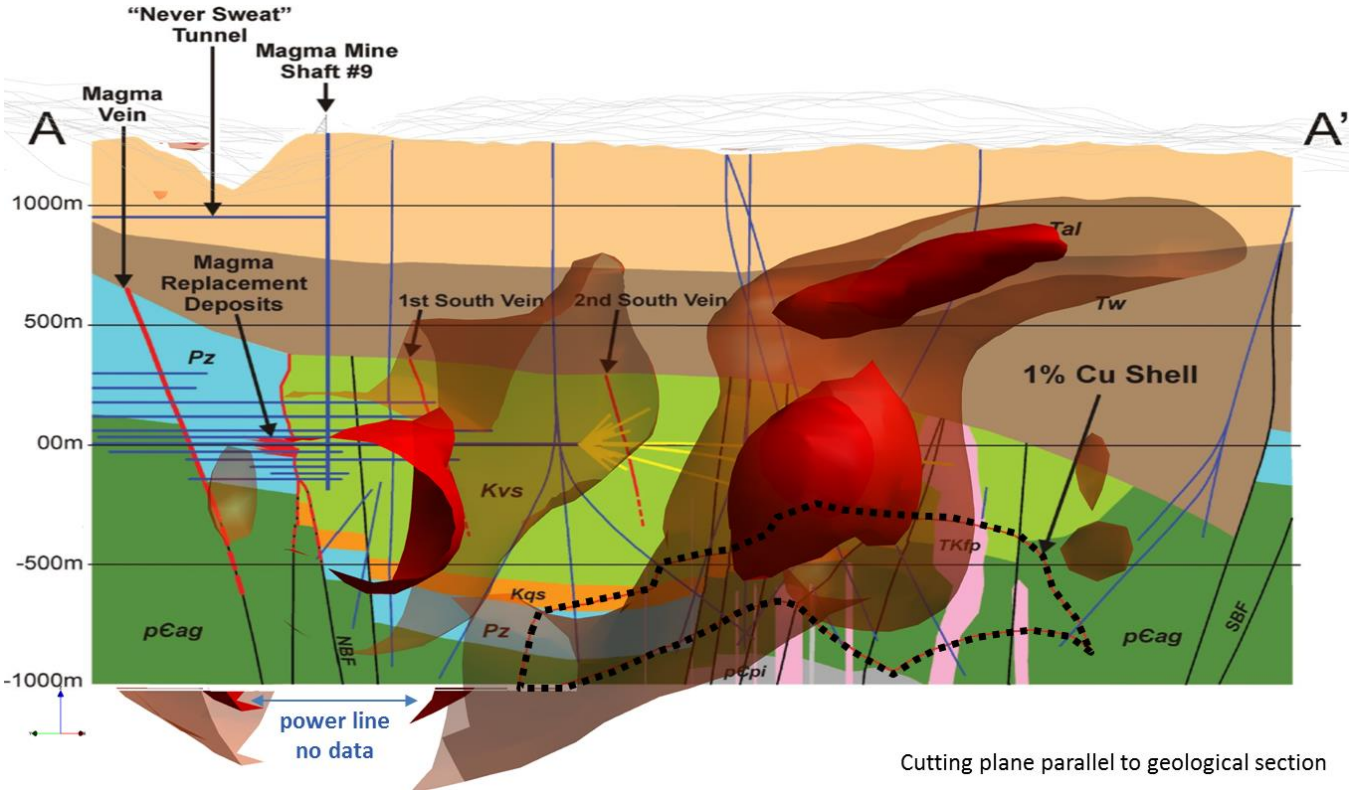

Figure 16a: ZTEM 3D inversion 15 and 30 mS/m (33 and 67 Ωm) conductivity isosurface shells from Figure 16b floating in front of the geological section from Resolution appears to display a reasonable correspondence between the elevated ZTEM recovered conductivity and the intensely pyritic zone between the 1% Cu shell and the overlying conductive sediments (after Witherly et al., 2016).

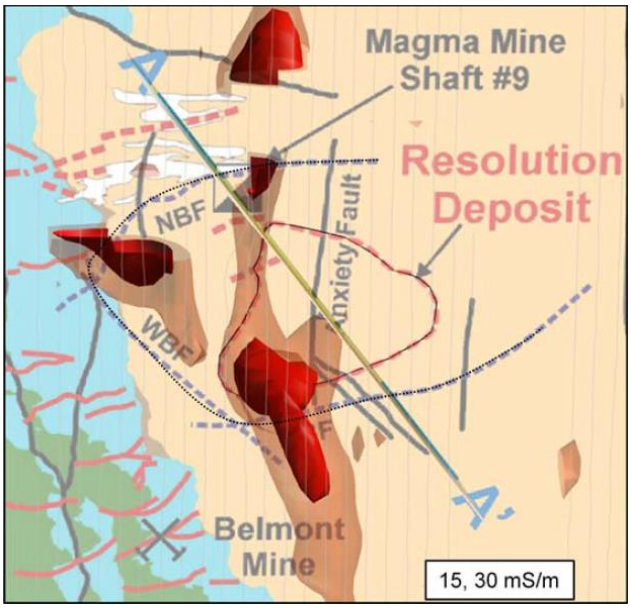

Figure 16b: Plan view of ZTEM 3D inversion 15 and 30 mS/m (33 and 67 Ωm) conductivity isosurface shells and Figure 16a geological section location (modified from Witherly et al., 2016).

The ZTEM 3D inversion performed by Witherly et al. (2016) exhibits surprisingly good results considering the amount of cultural noise affecting the data. By the skin depth rule, the 30 Hz minimum ZTEM frequency is clearly struggling to see through the conductive Whitetail conglomerate. Possibly a local thinning and/or less conductive facies of the Whitetail conglomerate is allowing the ZTEM response to poke through it, and could explain why only the southern end of Resolution appears to respond to ZTEM (Figures 16a and 16b). The shallower conductive blob, sneaking out of the deposit outline, appears to have some correlation to the overlying conductive sediments and structure, but the actual geological cause is unclear.

That ZTEM managed to pick up any hint of Resolution at ~1 km depth through conductive cover is in itself quite impressive. But this example also illustrates the limitations of the system as imposed by its 20–30 Hz minimum frequency and the fundamental inability for tipper data to distinguish the complete geological picture in layered geology.

Santa Cecilia, Chile

Santa Cecilia is a gold-rich porphyry deposit of Chile's Maricunga belt. The 24–22 Ma vertically elongated system is related to quartz diorite multiphase stocks that intrude into Oligocene to Miocene volcanics of the Aguas Blancas and Rio Nevado Formations (Moreno and Gibbons, 2007). Mineralization is hosted primarily in gold-bearing stockwork

and sheeted-vein ores. Sulphides are dominated by pyrite, with minor chalcopyrite and traces of bornite and molybdenite.

A CSAMT survey carried out in 2010 acquired data across a 2–9000 Hz bandwidth but only those frequencies >24 Hz were deemed usable because the proximity of the transmitter negated the plane-wave assumption for the lowest frequencies. Although the far-field limitation only allowed for a 750 m depth of investigation, this proved sufficient to illuminate a horseshoe shaped conductor that was subsequently drilled in 2011 to return approximately 0.2 g/t Au, 0.25% Cu, and 80 ppm Mo over 1000 m (Bournas and Thomson, 2013).

This exploration success prompted the commissioning of a more extensive and sophisticated survey in 2012. The 3D DCIP/MT survey utilized 50 "Orion 3D" Distributed Acquisition Units (DAUs) developed by Quantic Geoscience Ltd. to log time-series voltage data from 300 receiver dipoles and used 539 current-injection points to acquire over 150,000 DC resistivity and IP data from the distributed array. A further advantage of such systems is that during quiescent periods between current transmits and at night, the DAU continues logging the natural field data "for free", if one charges the survey set-up cost to the DCIP survey. At Santa Cecilia, the survey acquired 100 MT sites with a bandwidth of 0.0001–50 Hz utilizing the same IP receiver dipoles, although with a sparser set of horizontal magnetic induction-coil positions (Bournas and Thomson, 2013).

Figure 17 compares a DC Resistivity section model, whose depth of investigation is confined to the top kilometre, with the 3D MT model, as constructed from data whose lowest frequencies probe down to many kilometres and for which the model depth cut-off is limited only by the survey extents. The 2012 DC conductor matches with the 2010 CSAMT conductor that was tested to return the encouraging mineralization. Although DC resistivity was adequate to locate the Santa Cecilia target, in hindsight MT showed the bigger picture. Therefore, if the goal is to discover mineral systems rather than to bump hunt for anomalies, the merit in using natural field EM methods to illuminate the deep-seated mineral system footpath is clear.

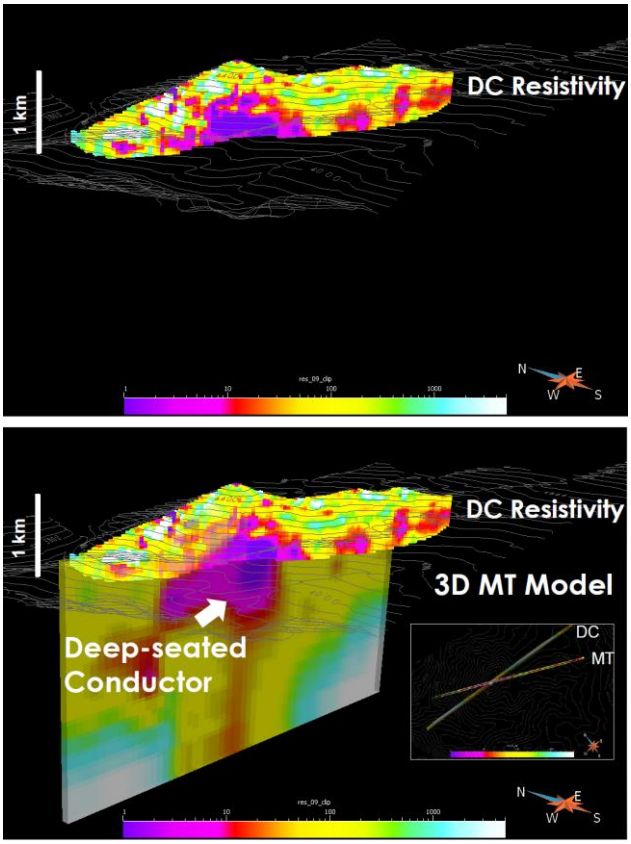

Figure 17: DC Resistivity 3D inversion model from Santa Cecilia [above], and the resitivity combined with a vertical slice from the 3D MT model [below] (after Bournas and Thomson, 2013).

Joint MT-ZTEM Inversion

With the ability of airborne ZTEM measurements to sample large areas quickly and cost effectively, and of ground MT to accurately measure the resistivity structure of the ground to greater depth, an obvious next step is to jointly invert ZTEM and MT data simultaneously. Recent publications discussing this are Sasaki et al. (2014), Sattel and Witherly (2015), Alembaugh et al. (2016) and Lee et al. (2017).

Sasaki et al. (2014) present the results of a detailed synthetic modelling study and concluded that "…inversion of sparse AMT data was shown to be effective in providing a good initial model for ZTEM inversion. Moreover, simultaneously inverting both data sets led to better results than the sequential approach by enabling [the identification of] structural features that were difficult to resolve from the individual data sets."

Sattel and Witherly (2015) compared 2D E- and B-polarization inversions with results from the 3D inversion code described in Holtham and Oldenburg (2010) from an area with both ZTEM and MT surveys, inverting each data set individually and jointly. They concluded that "…joint inversions can [successfully extract] the combined subsurface conductivity information from the two data sets." Most recently, Alembaugh et al. (2016) used Key's (2012) code to produce 2D inversions over a potential CO_2 reservoir in the northern Raton Basin of southern Colorado, USA. The challenges they encountered in reconciling 3D structure with a 2D inversion code are discussed in their text.

However, the most detailed discussion of the benefits and challenges of jointly inverting MT and ZTEM data is provided in Lee (2015) and Lee et al. (2017) using data collected over the Morrison porphyry-Cu deposit in British Columbia, Canada. In particular, the unpublished M.Sc. thesis documents five major challenges that need to be tackled when jointly inverting data:

1. Data rotation: ZTEM is collected using an XYU convention where X is along the flight line in the direction of travel with Y orthogonal to X in the horizontal plane such that Z is up, while MT has historically been collected in an NED (north, east, down) convention. It is imperative to reconcile both data to the convention of the code being used;

2. Data down-sampling: A ZTEM survey may contain thousands of data that will swamp the results of the tens of MT stations typically collected. Holtham (2012) introduced a weighting function to account for this discrepancy based on the number of stations N of each data type acquired:

$$\gamma = N_{ZTEM} \,/\, N_{MT} \tag{9}$$

3. Mesh generation: The final model-space discretization must combine the resolution of both surveys, which is especially challenging in areas with significant topographic relief;

4. Galvanic distortion: Affected data must be appropriately addressed; and lastly,

5. Model reconciliation: The MT-derived resistivity should agree with the best-fit starting-model of the ZTEM data.

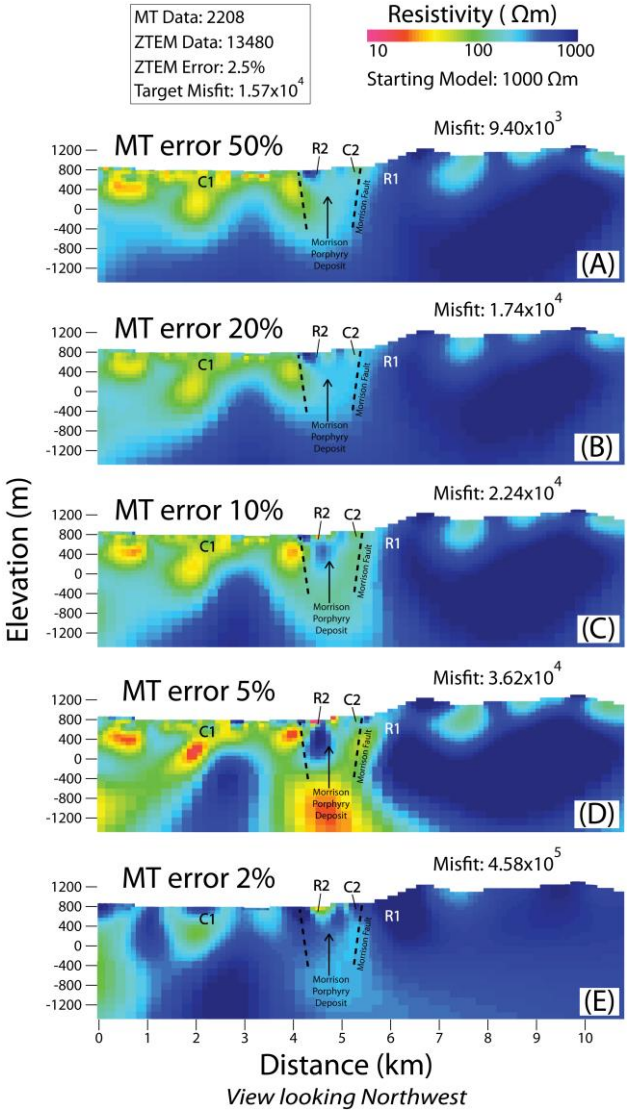

Figure 18: Morrison joint inversion results (modified by Lee from Lee, 2015). From top to bottom the panels show the effect of gradually increasing the weighting of the MT data.

Morrison, British Columbia

Although not nearly as well-endowed as most of the other porphyry deposits discussed herein, Morrison is included because it represents the best documented example of a joint MT-ZTEM inversion for porphyry-Cu exploration.

Lee (2015) and Lee et al. (2017) examined ZTEM and MT data collected over the Morrison Cu-Au-Mo deposit in the northern Babine Lake region of British Columbia. Morrison is genetically and spatially related to an Eocene plagioclase–hornblende–biotite porphyry stock that intruded into the Middle-Late Jurassic Bowser Lake Group sediments (Liu et al., 2016) and represents a typical example of a calc-alkaline porphyry system in British Columbia. The advanced stage project proposes an open-pit mining operation to develop proven and probable reserves of 224 Mt with an average grade of 0.330% Cu, 0.163 g/t Au and 0.004% Mo (Wardrop, 2009).

The ZTEM data over Morrison were acquired in 2010 at a line spacing of 250 m with six frequencies from 30–720 Hz, while the MT survey comprised 37 stations collected in 2013 with a nominal station spacing of 500 m over the deposit, expanded to ~1 km further afield. The bandwidth of the MT data was 0.001–300 Hz and the acquisition included ground tipper data allowing for a direct comparison with the ZTEM tipper data (Lee et al., 2017).

Figure 18 shows five common vertical sections through Morrison testing different weightings between the ZTEM and MT data in the joint inversion. The input data consisted of 13,480 ZTEM data and 2,208 MT data. The ZTEM was given a constant error of 2.5% while error on the MT data varied between 50% (low influence) and 2% (high influence). At 50%, the ground data have little effect on the inversion and the result is essentially the same as the ZTEM only inversion, while at 2% the joint inversion is unable to fit both data sets simultaneously. Lee et al. (2017) concluded that, in this case, 10% error was the most reasonable.

Sediment Hosted Copper

Following porphyry deposits, sediment hosted copper deposits are the world's second most important source of copper, accounting for ~15% of the global copper inventory (Sillitoe, 2012). The Central African Copperbelt, stretching across Zambia and the Democratic Republic of the Congo (DRC) and into Angola, is the world's largest and highest grade sedimentary copper district and also contains the world's largest reserves of cobalt (Hitzman et al., 2012). For the greater part of the past century, rigid acceptance of a syngenetic model largely constrained Copperbelt exploration to certain stratigraphic units, the Zambian Lower Roan and the Congolese Série des Mines, which were believed to be the sole ore bearing strata of economic significance (Mendelsohn, 1961).

That constraining hypothesis was spectacularly disproven in 2006 by the discovery of the giant Kamoa deposit outside of the generally accepted Copperbelt margins and far above the traditional ore bearing stratigraphy (Broughton and Rogers, 2010). Other modern discoveries in Zambia's North-Western Province, as well as Frontier in DRC, add to the tally of major

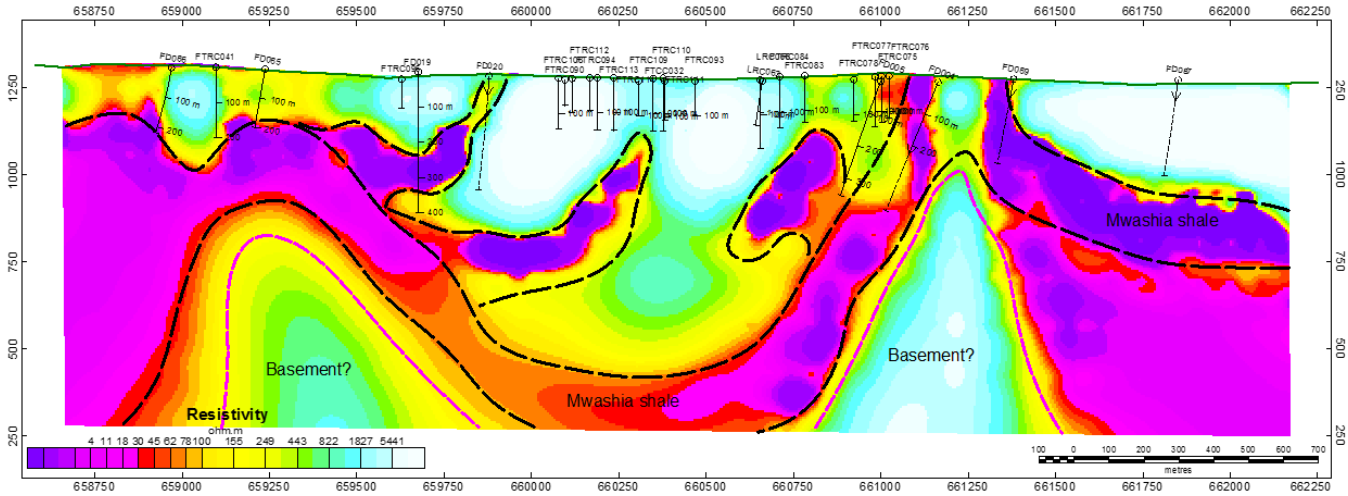

Figure 19: AMT 2D inversion section near Frontier Mine in DRC (modified from Wijns, 2013).

resources outside the traditional Copperbelt pay-zones and form a mounting body of evidence that the potential of any stratum to host ore lies only in its position relative to basement and its capacity to serve as a redox trap, either as a red bed host to mobile paleo-hydrocarbons or as an in-situ carbonaceous reductant.

Copperbelt exploration-geophysics has been revitalized by this realization that any reducing unit can potentially host mineralization and geophysics is being applied to map the fluid pathways and the reducing traps that comprise sedimentary copper mineral systems. In particular, natural field EM methods are proving to be a powerful tool due to their ability to illuminate the stratigraphic and chemical architecture conducive to forming giant deposits across scales ranging from entire basins to drill targets. Hitzman et al. (2012) concluded that, "exploration for Central African Copperbelt-type bodies shares many similarities with the search for petroleum. Given this fact, seismic and/or the inversion of potential fields and electrical data to constrain subsurface geology may become common exploration techniques in the coming decades." In 2017, that decade has arrived.

Frontier, DRC

The 2D AMT section of Figure 19 illustrates the premise of using AMT to target the lowermost reducing horizon above the basement, which is in this case the Mwashya shale, at potential structural trap sites for mineralizing fluids focussed towards the dome apices. It is important to note that the AMT data was only acquired after a substantial amount of drilling had already occurred along this section. Unfortunately, the drill hole assay results have not been released for comparison, but had the AMT survey been collected beforehand the drill pattern would surely be different (C. Wijns, pers. comm.).

Kansanshi, Zambia

FQML's interest in structural domes can be well understood by looking at their flagship Kansanshi asset, which in partnership with ZCCM International Holdings PLC is one of Africa's largest and most productive high-grade copper mines. The deposit is located in North-Western Province, far outside the historical Zambian Copperbelt, and its ore is hosted by Mwashya–Grand Conglomérat intervals far above the traditional Copperbelt ore-bearing stratigraphy (Hitzman et al., 2012). As Figure 20 illustrates, the high-grade Kansanshi mineralization occurs predominantly as undeformed high-angle vein swarms along the crest of the Kansanshi antiform (Broughton and Hitzman, 2002). The high-grade veins are most abundant near parasitic domes that bestow extra flexure on the main Kansanshi dome, making the targeting of "domes-on-domes" an apt tagline for an effective exploration strategy (Wijns, 2013).

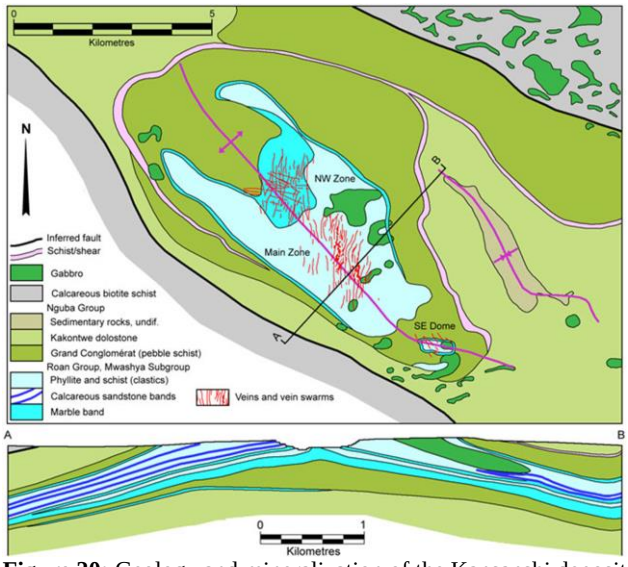

Figure 20: Geology and mineralization of the Kansanshi deposit (after Hitzman et al., (2012), Gregory et al. (2012); and sources cited therein).

Figure 21 shows the results of an AMT traverse across Kansanshi where the conductive layer of the 2D inversion model corresponds to the carbonaceous phyllites of the Mwashya group, which hosts much of the mineralization, and illustrates the doming geometry thought critical to focusing the high-grade

veins. As with porphyries, Kansanshi illustrates the ability of natural field EM methods to guide subsurface targeting based on an understanding of the mineral system.

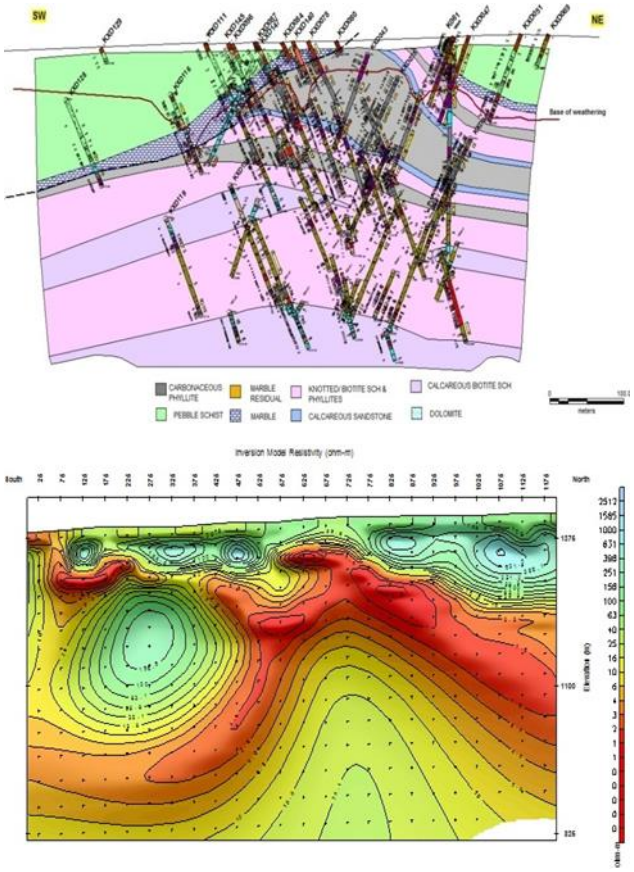

Figure 21: Kansanshi geological section [above] and AMT 2D inversion resistivity model [below] (after Wijns, 2014). Correlation between the AMT conductive layer and the carbonaceous phyllite is evident despite the sections are not exactly collinear and there is some difference in their scaling.

Magmatic Ni-Cu-PGE

Voisey's Bay, Newfoundland and Labrador

The Voisey's Bay deposits (Ovoid, Eastern Deeps, and Reid Brook Zone or Western Extension) are the result of a discovery made by two prospectors in 1993, who fortuitously deployed a heavier geological-hammer on the Discovery Hill gossan than government geologists had utilized some years prior, thereby breaking off a larger sample that contained visible sulphide mineralization. Voisey's Bay is thus an EM-discovery story, beginning with those two prospectors who used high-frequency, visible spectrum EM radiation to identify the gossan (King, 2007), followed by a variety of ground and airborne EM systems. And between an MT surveys acquired in 1996 and 1997 followed by ZTEM in 2007, Voisey's Bay provides a natural field EM example of an extremely high conductivity-thickness orebody.

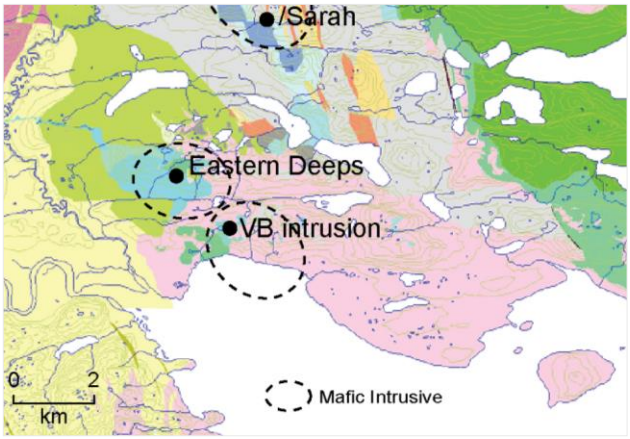

Figure 22: Voisey's Bay Main Block geology showing main mafic intrusive bodies (after King, 2007, courtesy Vale Canada Limited).

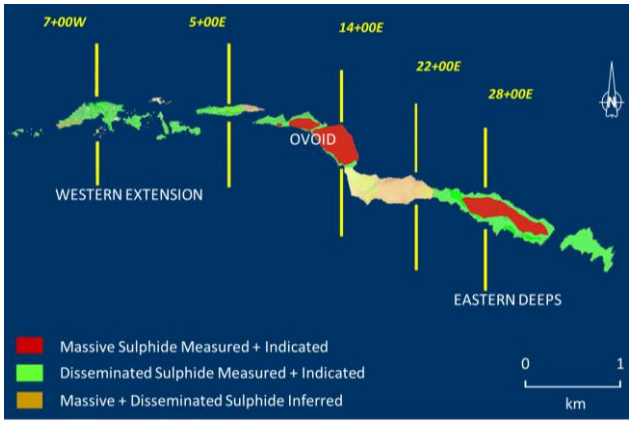

Figure 23: Plan view of the three Voisey's Bay deposits (Balch et al., 1998).

All the deposits are hosted by troctolite dikes thought to be feeder conduits for the Reid Brook intrusion of the Nain Plutonic Suite (Balch et al., 1998). In typical magmatic sulphide fashion, the Eastern Deeps mineralization settled into topographic lows in the magma chamber, while brittle host rocks of the Ovoid and Reid Brook Zones created the space required to host the ore. In 2003, the total reserve plus resource estimate by then-Inco for the three deposits was about 141 Mt grading 1.63% Ni, 0.85% Cu and 0.09% Co (Kerr, 2003). The orebodies range in depth from under ~20 m of cover for the Ovoid to 800 m deep for the Eastern Deeps Zone. Figures 22 and 23 present the local geology and a plan view of the deposits respectively.

The first active source geophysical survey employed was horizontal loop EM (HLEM), whose frequency is a full 12 orders of magnitude lower than that of visible light, delineated the conductive zone corresponding to the Ovoid. Subsequently, other active-source EM systems were employed, including distant-source (VLF), frequency-domain helicopter EM (DIGHEM), time-domain fixed-wing (GeoTEM), time-domain large-loop step-response (UTEM), time-domain large-loop impulse-response (Crone and EM-37) plus both time-domain impulse- and step-response borehole surveys (Crone and

UTEM), all of which displayed significant responses owing to the orebody (Balch et al., 1988).

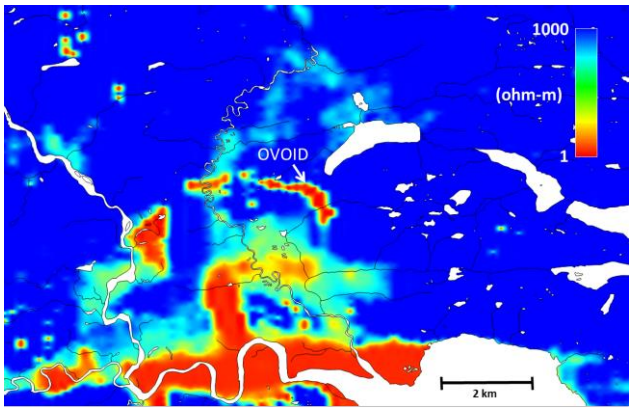

Figure 24a: HEM CP 900 Hz (after Balch, 1999).

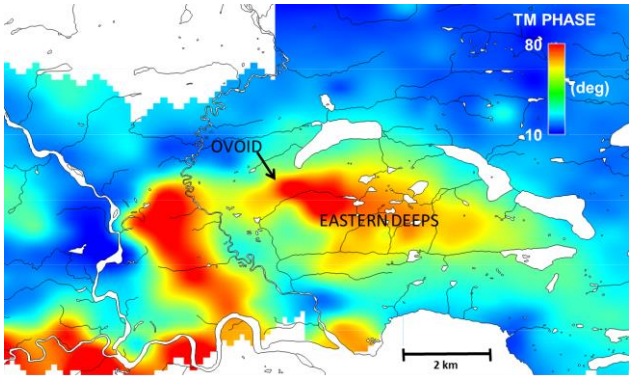

Figure 24b: AMT TM-mode (B-polarization) impedance phase (after Balch, 1999).

Natural field EM data were first collected regionally in 1997 along 14 × 13 km long north-south lines spaced 800 m apart using a 4-channel EMI receiver over a frequency range of 10–10,000 Hz. The 100 m spaced stations consisted of two horizontal B-field coils and two horizontal 50 m long E-field field dipoles. The AMT profiles over the deepest portion of the Eastern Deeps deposit clearly showed a marked drop in apparent resistivity to <1 Ωm. Even farther to the east over the Far East Zone, the AMT profiles exhibited zones of low apparent-resistivity that were subsequently confirmed to be sulphide mineralization at depths near 1.5 km (Balch et al., 1998). The location of Voisey's Bay between two fjords presented processing challenges because the background conductivity changed from 3.3 S/m conductive seawater flanking the lines to >10,000 Ωm country rocks cropping out in the centre.

Figures 24a and 24b compare plan-view representations of the lowest-frequency co-planar DIGHEM HEM data and the AMT TM-mode impedance phase data for an unknown frequency. As expected, the near-surface Ovoid deposit only shows up in the HEM data, while not unsurprisingly the deeper Eastern Deeps deposit is only apparent in the AMT data. The difference is mainly related to the relatively low-power of the DIGHEM system, rather than a skin-depth argument. Some skepticism has been directed towards the interpretation of the 2D TM-mode inversion over the Eastern Deeps because of artifacts that appear at contacts, as shown in Figure 25: is the anomaly related to the deposit or simply a geological contact? However, the combined 2D TE+TM inversions shown in Figure 26 do a much better job imaging the Eastern Deeps deposit (Watts and Balch, 2000).

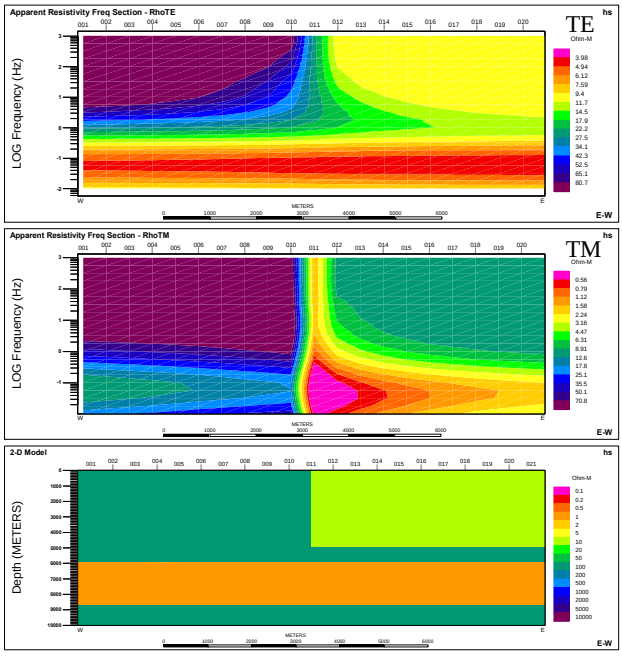

Figure 25: A simple 2D geoelectric model (below) with its TE (top) and TM (middle) response versus frequency. The 100 Hz is highlighted with the black line. The TE response does a reasonable job in recovering the starting model, while the TM mode shows a spurious response at the location of the vertical contact, and below at the lower frequencies mapping the lower conductive layer (courtesy B-Field Geophysics Ltd.).

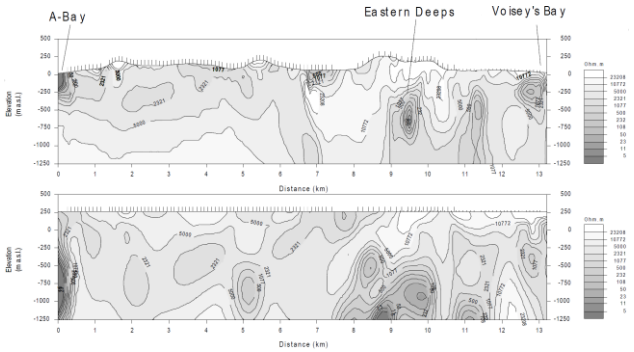

Figure 26: Constrained (above) and unconstrained 2D AMT inversions along line 572 (Watts and Balch, 2000).

The unconstrained inversion used a uniform half-space starting model with no topography and approximately indicates the position of the conductor associated with Eastern Deeps mineralization while also showing possibly spurious structures in areas with data gaps (e.g. at 8 km). By using HEM data to fix the near-surface conductivity of some elements in the starting model, including sea water on the edges, the constrained inversion presents a more compact and realistic Eastern Deeps

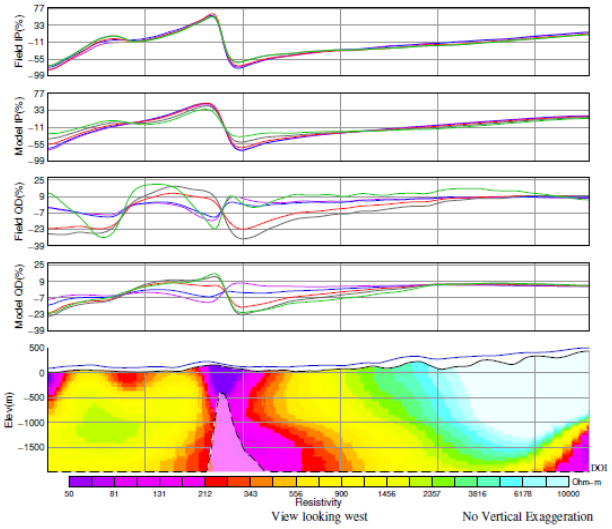

Figure 27a: ZTEM profile over the Reid Brook Zone. Panels from top to bottom are: in-phase response, modelled in-phase response, quadrature response, modelled quadrature response, and the 2D inversion using only T_zx (the in-line component), which assumes TE mode or E-polarization, an important concept to understand. The dashed line in the bottom shows the depth-of-investigation (DOI) limit. The clear cross-over in the tipper with limited in-phase amplitude change between the frequencies shows that the Reid Brook Zone is an excellent conductor, but the response is mainly sampling the mildly conductive dyke outcropping on surface. The highly-conductive main deposit at depth is below the DOI (courtesy Vale Canada Limited).

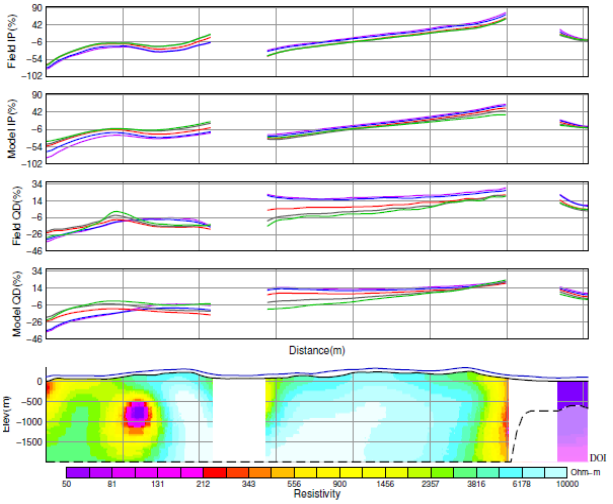

Figure 27b: ZTEM profile over the Eastern Deeps. Here the cross-over is much less pronounced, and is perhaps greater in the quadrature component. Although difficult to envisage an anomaly, the 2D T_zx inversion does an excellent job in positioning the Eastern Deeps in the correct location and at the correct depth (courtesy Vale Canada Limited).

deposit. But although the geometry of the deposit is better, its modelled resistivity is only <5 Ωm, far too resistive based on the 10^7 S conductance of the Ovoid (King, 2007). This poor resolution of the magnitude of the physical property is typical for all band limited EM surveys over extremely high conductance targets.

Theoretically, the inductive limit of a step-response system like UTEM is $V_{STEP}(t) \propto e^{-t/\tau}$, where $V(t)$ is the secondary voltage due to a discrete conductor with time-constant τ at time t after the transmitter is turned off. Correspondingly, the response of an impulse-response system is the time-derivative of the above and is thus scaled by a factor of $1/\tau$, such that $V_{IMP}(t) \propto 1/\tau\, e^{-(t/\tau)}$. A time-domain impulse-response airborne system will thus have problems determining the true value of high-conductance targets. Broadband natural field systems should theoretically not suffer from that problem, but ZTEM is not broadband. Regardless, a trial ZTEM survey was commissioned in 2007, one of the earliest. Selected results are shown in Figure 27 over the Reid Brook and Eastern Deeps zones. Unfortunately, data collected over the Ovoid were unusable because of power line noise.

The Reid Brook profile highlights a text book crossover from the induced field of the highly-conductive vertical plate that is the deposit. The lack of decay in the in-phase profiles from 360 Hz down to 30 Hz is a testament to the quality of the main conductor that lies at 400 m depth, while the quadrature response is seeing the less conductive portions of the dyke that extend from the deposit to the surface. In contrast, the profiles over the Eastern Deeps display at best a subtle anomaly that would be difficult to convincingly interpret as a target, and yet the 2D T_{zx} inversion is very focussed and located at the correct depth. What is likely is that the Eastern Deeps response is due mainly to current channeling while the conductive vertical-plate at Reid Brook may have an induced component as well.

Unconformity-Associated Uranium

With average grades of ~2% U and large deposits of exceptional grade like McArthur River at over 22% U, the Athabasca Basin of northern Saskatchewan, Canada is the world's most exciting uranium play. The Athabasca uranium story began in the late 1960s when the Dynamic Group of Calgary-based oil and gas companies recognized its similarity to other Proterozoic quartzarenite basins where sandstone-hosted U deposits had been discovered. They proceeded to apply the highest frequency natural EM field, gamma rays, to survey the entire basin with an airborne total-count natural-gamma detector. A radioactive boulder train was traced back to Rabbit Lake, where drilling soon intersected a new type of deposit with U grades far surpassing anything ever yet seen (Schiller, 1978).

Natural-gamma surveying to map boulder trains proved effective for finding shallow, <200 m, deposits eroded by glaciers, which lead directly to the discovery of the Key Lake deposits in 1975–76 (Kirchner and Tan, 1994). The Key Lake deposits were very influential to subsequent exploration in the Basin because this is where the relation between uranium mineralization and post-sandstone reactivated graphitic faults was first recognized (Schiller, 1978), and with advances in

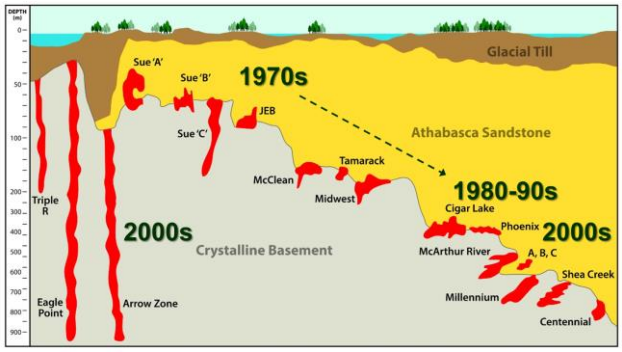

Figure 28: Progression of deepening deposit discoveries in the Athabasca Basin (modified from Thomas, 2015). Note the vertical scale change at 200 m.

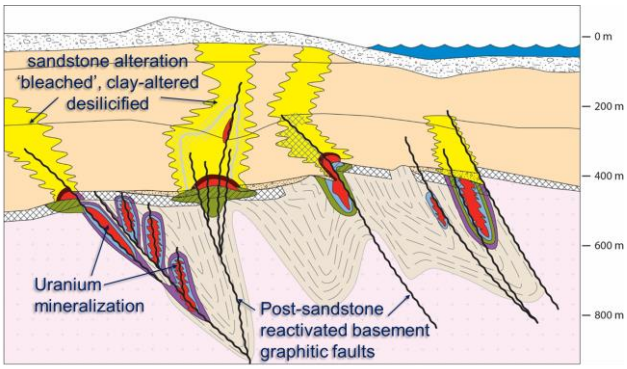

Figure 29: Generalized model for an unconformity-associated uranium system footprint with various deposit styles and main features that can be targeted at a distance by geophysics pointed out (modified from Thomas, 2015).

large-loop TEM systems, these structures could be mapped to depths exceeding 600 m. Faced with diminishing prospects for finding deposits with any form of surface expression, the geophysically-driven strategy that Key Lake inspired to systematically drill to the unconformity along conductor subcrop axes mapped with controlled-source EM methods soon led to discovery of both the giant and incredibly high grade Cigar Lake and McArthur River deposits in 1981 and 1988 respectively, and cemented that strategy as the general recipe for subsurface exploration of the basin in decades following (Gandhi, 1995).

More recently, explorers have come to realize that significant uranium mineralization does not have to occur immediately at the unconformity on the basement conductor subcrop. The Millennium discovery of 2000 proved that sizable high-grade deposits can occur within the basement and several hundred metres off the conductor axis as well. This realization has prompted companies to take a more integrated approach, where geophysics is utilized more generally to image subsurface geology, rather than exclusively as a tool to hunt for anomalies (Cristall and Brisbin, 2006). The progression of exploration towards deeper parts of the Athabasca Basin, as illustrated in Figure 28, is a trend that is expected to continue. Fortunately, a continually improving understanding of the unconformity-associated uranium mineral system, together with technological developments in deep 3D geophysical imaging and modern, integrated targeting practices centred on predicting geology from geophysics bodes well for future Athabasca Basin discoveries.

Various deposit styles can arise depending on the particular fault-architecture that focussed mixing between ingressing uranium-laden hypersaline sandstone fluids and egressing hydrothermal basement fluids (Fayek and Kyser, 1997) in proximity to the uniformity that separates the oxidized sandstone and reduced basement environments. Figure 29 illustrates styles ranging from the classic sub-horizontal cigar shaped orebody sitting on the unconformity at a post-sandstone reactivated basement graphitic fault with a huge argillic-alteration plume extending into the sandstone (e.g. Cigar Lake), to the basement-hosted, vertically-elongated, tabular ore bodies occurring in hanging wall faults (e.g. Eagle Point). While each deposit style has its own unique characteristics, in general they share commonalities in terms of close associations with post-sandstone reactivated basement graphitic fault networks and varying degrees of hydrothermal alteration, which commonly include sizable zones of de-silicified and clay-altered sandstone (Thomas, 2015).

McArthur River, Saskatchewan

As part of the EXTECH-IV research project (Craven et al., 2002), an AMT survey was collected in 2000 and 2001 at McArthur River, the world's richest uranium mine with ore zones at depths between 500–650 m. The survey objective was to evaluate the capability of AMT to map deep-basement graphitic fault-conductors as well as alteration-related resistivity variations in the overlying sandstone. The survey comprised 135 stations acquired along 11 profiles oriented perpendicular to the P2 fault structure on which the deposit is situated. The nominal line- and station- spacing was 800 m and 300 m respectively. Post-processing included the application of digital comb-filters tuned to remove harmonic noise from the mine and robust remote-reference techniques (Larsen et al., 1996) to recover minimally-biased transfer functions from which smoothly varying apparent resistivity and phase curves covering the frequency range from 3–10,200 Hz were derived (Craven et al., 2002).

Tuncer et al. (2006) applied the Non-Linear Conjugate Gradient (NLCG) algorithm of Rodi and Mackie (2001) to invert the data in 2D and used Siripunvaraporn et al.'s (2005) code to invert the data in 3D. Comparing the models to five available borehole resistivity logs (not presented herein) showed the best agreement with the combined TE-TM-T_{zy} 2D inversion model of Unsworth et al. (2006) (see Figure 30), a result supported by dimensionality analyses indicating the data were largely 2D. The figure provides a relevant overall summary of the work, which succeeds in imaging the P2 conductor at a resolution proportional to the imaging depth. More generally, it provides an excellent illustration of the superior imaging that can be achieved by combining data that measure five components of the natural EM field $(E_x, E_y, H_x, H_y, H_z)$ and utilizing the inherently higher resolution E-field data that can only be acquired on the ground, as opposed to surveying only for tipper (T_{zy}) data.

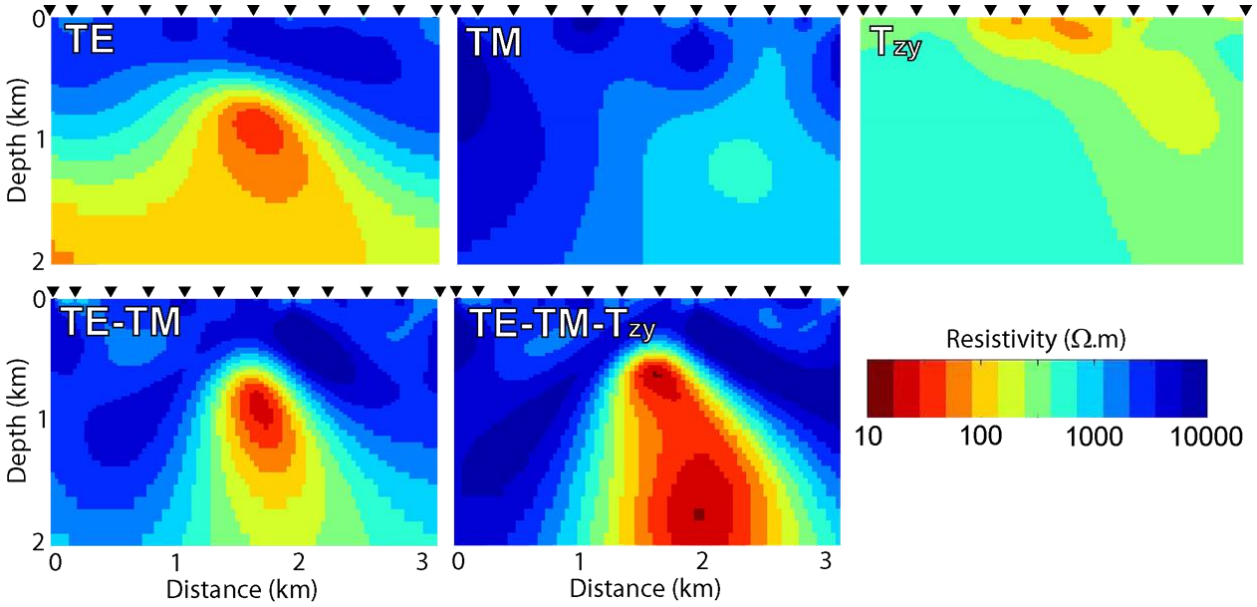

Figure 30: 2D inversions of various components of the McArthur River AMT data, individually and together, showing that superior imaging is achieved when both TE and TM modes, or E- and B-polarizations, are combined with tipper (T_zy) magnetovariational sounding data (after Unsworth at al., 2006).

Farquharson and Craven (2009) expanded on this work, taking a purposefully direct approach of inputting the complete impedance tensor, in its un-rotated acquisition coordinates, directly into a 3D inversion without any form of statics shifting or other pre-processing. The 3D inversion program utilized was that of Farquharson et al. (2002), a minimum-structure Gauss-Newton algorithm that formed the prototype to all the later UBC natural fields EM 3D inversion codes as discussed earlier. With the computational resources of the time, a subset of 11 frequencies ranging from 3.8–1280 Hz were inverted on a 3D mesh with *x*-y cell dimensions of 200 m × 200 m in the core mesh region. Figure 31 illustrates the 3D inversion result.

Although not fully appreciated at the time, this pioneering work offered an early glimpse of the potential for 3D inversion of natural fields EM data and helped influence a paradigm shift in subsurface exploration in the Athabasca Basin from chasing geophysical anomalies to imaging the complete unconformity-associated uranium mineral system, as per McCuaig and Hronsky (2014). Moreover, it foresaw that with ever increasing availability of affordable computer hardware, 3D MT inversions would become tractable in mineral exploration, thus eliminating the dimensionality limitations of 1D and 2D inversions and their associated interpretation challenges.

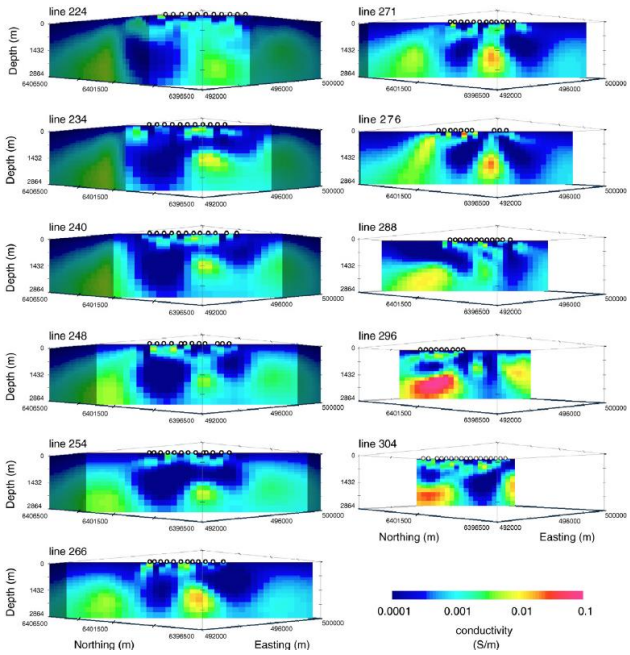

Figure 31: Vertical slices through McArthur River 3D AMT inversion model (after Farquharson and Craven, 2009).

Greenfield and Blue Sky

The Transient AMT (TAMT) approach using adaptive polarisation stacking, as described by Goldak and Goldak (2001), is well suited to acquiring natural field EM data through frequencies ranging between the ELF band (3 – 30 Hz) through to the VLF band (3–30 kHz). The high frequency data, typically up to 32 kHz for TAMT as compared to 10 kHz for conventional AMT systems, is a key advantage for resolving statics effects arising when E-field dipoles span conductive bog and resistive till, which can have resistivities differing by as much as five orders of magnitude. In turn, this improves depth imaging in parts of the basin where both the glacial-till overburden and underlying Athabasca Group quartzarenite are very resistive (~10,000 Ωm). Surveys at Virgin River (Leppin and Goldak, 2005), Millennium, and La Rocque Lake (Powell et al., 2007) have consistently demonstrated, with results confirmed by drilling, that TAMT successfully images both

basement graphitic conductors and hydrothermal alteration chimneys in the Athabasca Group sediments, albeit at resolutions limited by the wide station- spacing of these surveys.

The value of an airborne system capable of simultaneously mapping deep, strike-extensive basement conductors and potential alteration zones in the overlying thick sandstone package is well appreciated and explains the rapid uptake of ZTEM in the Basin. The example shown in Figure 32 illustrates the complementary information contained in the lower frequency ZTEM data, which can trace the basement graphitic faults in good agreement to the conductor axes historically mapped using ground TEM, and the high frequency ZTEM data, which identifies cross-cutting structures and possible hydrothermal alteration zones in the Athabasca Group sediments. The idea of consistent spatial coverage across such a broad area is highly appealing to those who have tried to traverse such distances on foot in the basin.

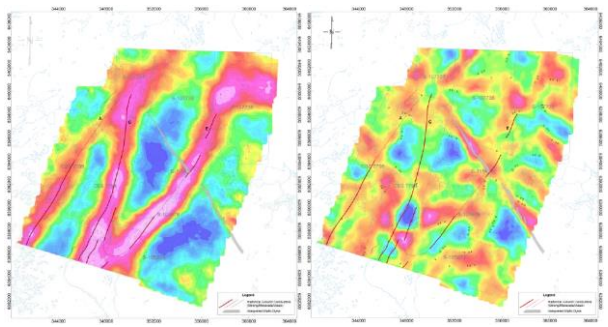

Figure 32: Conventional ZTEM DT images from the Athabasca Basin with 30 Hz data [left] showing good correspondence to basement conductor traces as mapped historically with ground TEM, and 720 Hz data [right] indicating cross-structures and possible argillic alteration zones in the Athabasca Group sediments (courtesy Cameco Corporation and AREVA Resources Canada Inc.).

DISCUSSION

Many successful exploration teams have applied their skills in observational geoscience and knowledge of porphyry mineral deposits to great commercial success, inspiring a generation of field geologists to prospect outcrops throughout the world's porphyry belts in the search for the next economic deposit. While the success of generations of boots-and-hammer geologists has provided most of the world's currently producing copper mines, they have also left a considerable opportunity for a new generation of explorers empowered with an evolving understanding of the mineralogical, geochemical, and geophysical signatures of the porphyry mineral system and who have at their disposal the modern technologies required to expand the search space deep beneath the surface.

The porphyry case studies presented herein with airborne ZTEM data outnumber ground MT examples simply because the former have been more widely publicized over the past decade. Mineral explorers take great interest in methods that can cover large areas quickly at relatively low cost and tend to view airborne methods as the logical technological progression from equivalent ground methods. Calc-alkaline porphyry-copper systems, like the ones presented, are also blessed with cubic kilometres of alteration (i.e. broad mineral-system footprints), such that even though the contrast between the altered and unaltered rock may be low, the sheer volume ensures that tellurics get channelled into those features. Further published work over alkalic systems will contribute greatly to this atlas of natural field responses.

However, with respect to ZTEM and MT, the reality is the two methods are not equivalent. By incorporating E-field information, MT is effectively an ohm-meter that is sensitive to the absolute conductivity of a variable background host including layered geology, while also adding tremendous sensitivity and resolution in the imaging of lateral contacts. Add the much lower frequencies it collects, typically down to ~0.001 Hz for sites left to record overnight, and there is no comparison to ZTEM's 20 Hz limit. Low-frequency data are compulsory for deep imaging in conductive hosts or overburden. Still, the significant benefit that ZTEM provides with its lower cost, high-density spatial sampling of the vertical magnetic component of the natural EM field to map lateral conductivity contrasts is impressive. The theoretical merit is clear, and 3D inversion workflows are increasingly being applied that combine ZTEM with MT to utilize all five components of the natural EM field: E_x, E_y, H_x, and H_y from ground surveys and H_z from ZTEM. These have already and will continue to demonstrate that the whole is far greater than the sum of its parts.

The Morrison example both highlights the benefits of jointly inverting dense tipper data collected from an airborne platform with sparse ground sites and prefaces the work that still needs to be done, being further technical research and exploration buy-in to collecting both data sets. To produce robust 3D resistivity images that span entire properties to kilometres depth is a major development in mineral exploration geophysics that may one day well prove to be on par with the advent of 3D seismics for oil and gas. Combined ZTEM/MT surveys are especially applicable in the Athabasca Basin, with its favourably resistive-background, where utilizing the lower frequencies of the natural EM spectrum to image the subsurface mineral-system footprint may one day rival the use of the high frequency, natural gamma, end of the spectrum that was used to explore its surface.

The progress from the initial near-surface discoveries in the Athabasca Basin to a rewarding period of undercover exploration presents an optimistic case for mineral exploration globally. Each new discovery utilized advancements in geophysical technologies that enabled successful integrated-targeting approaches, not dissimilar to the development of integrated targeting-culture in the petroleum industry. Similarly, through more than a century of prospecting in the Superior porphyry copper district in Arizona, the natural field EM signal from the deep Resolution deposit has always been present, only waiting for someone with the right equipment and know-how to listen for it. This and other case studies from Australia, Canada, Chile, USA, and Zambia serve to illustrate the vast opportunity that lays beneath our feet in greenfield areas and at depth within historical mining districts where we have only scratched the surface.

PREDICTIONS FOR THE NEXT 10 YEARS

The success of Geotech's ZTEM system suggests that other players will enter this space. This will not only spur innovation in both hardware and software (signal processing and data inversion), but the increased competition may drive down costs, benefiting explorers enormously. A ZTEM-variant called Airborne Magnetic Tensor (despite the confusing acronym) that measures the three-component H-field from an airborne bird was introduced by Geotech in 2009, to limited commercial success. Augmenting this system with ground remote referencing capabilities would be of great benefit to eliminate the current shortcomings inherent to using a single base station for both the competing requirements of local and remote referencing. Improved three-component receiver systems will most likely be developed, which if oriented would provide vector data, or if not would provide a total-field measurement, although that would need to be accompanied by new inversion capabilities.

Capacitive antennas have already been used by some companies (EMpulse Geophysics Ltd., and GroundMetrics, Inc., amongst others) and will continue to gain traction because of their ability to mitigate galvanic distortions in horizontal-component electric fields, in addition to even measuring the vertical component of the electric field at surface. Capacitive contacts also greatly simplify the practical challenges faced by traditional galvanic contacts in very rocky, dry, or ice- and snow-covered areas.

Of course, incremental improvements will continue to be made: less expensive hardware and a better understanding of the sampling density required to image an ore system will continue to encourage the acquisition of optimised survey data. The kinds of data will also change. In the future, more surveys will include a mix of multiple E-field only stations surrounding a few "common" offset H-field sites, full MT sites, and H-field only sites, the latter of which are acquired both on the ground and from the air. Optimizing the relative amounts of each data type will require modelling. Some groups have been thinking about using drones to ferry induction coils to magneto-only sites to generate tipper data (G. Heinson, pers. comm.).

Combining offset E-field and H-field sites will require modifying the inversion codes to allow for arbitrary positioning of coils and potential electrodes. Modelling the actual location of the H-field coil rather than simply transcribing it to each associated E-field measurement, as is typically done with EMAP-style surveys, will be a big improvement, especially in topographically challenging areas.

Rather than simply searching the smooth-model space, MT inversion codes will also continue to develop the functionalities required to include both hard- and soft-constraints. Hard constraints like overburden thickness, sedimentary basin thickness, ocean depth, and coastline definition, etc., are geological, while soft constraints focus on data- and model-norms.

Graham Heinson (pers. comm.) has suggested that more fundamental petrophysical research is required on the causes of conductivity variations in the deep crust. Some formations are obviously conductive (melt, shear zones from fluids, etc.); however, very little is understood about why the lower crust can be a conductive as seawater, and there has been virtually no research in this area for the last 20 years, which indeed suggests additional work is long overdue. This together with more large-scale airborne natural field surveys complementing sparser ground stations, along the lines of USArray (Meqbel et al., 2014) or AusLAMP being undertaken by governments or industry consortia will help close the loop.

CONCLUSIONS

That future exploration is going to take a mineral systems approach is reasonably assured as this framework provides structure to exploration in new areas and under cover, something that has perhaps been lacking in the past decade. McCuaig and Hronsky (2014) discuss the scale dependency of mineral systems, highlighting a natural and requisite change in focus from continental to province, camp, deposit, and finally down to the ore-shoot.

As is to be expected with the advent of new technologies like ZTEM and MT (at least relatively "new" to mineral exploration), both methods were "trialed" over numerous deposits in the past 10 years to confirm their effectiveness. The examples presented in this paper show the utility of natural field EM methods in IOCG, porphyry and sediment-hosted copper, Athabasca-style uranium, and magmatic Ni-Cu-PGE mineral systems. Given that natural field EM methods can image the crust's geoelectric structure across a variety of scales, which explorers can interpret to locate mineral systems and vector to deposits, these techniques can now confidently be included in the exploration toolbox. In mineral exploration, the future will belong to those with skills to use all the tools in the box to map mineral systems, and knowledge of how best to use natural field EM methods will be key.

ACKNOWLEDGEMENTS

Firstly, we would like to acknowledge our employer, Anglo American plc, for supporting the writing and presentation of this paper. We would like to acknowledge the organising committee of DMEC *Exploration'17*, and especially the leadership of Alan King, Chair of the Near-Mine and Camp-Scale Exploration session, who invited us to prepare this review. Data and figures were willingly provided by Anglo American plc, Cameco Corporation and AREVA Resources Canada Inc., CODELCO, FQML, Geotech Ltd., and Vale Canada Limited. We greatly acknowledge the huge contribution their data has made to this paper, because it is through their examples that mineral exploration will continue to evolve. Therefore, the entire mining fraternity is indebted to them. And finally, we acknowledge the highly enlightening conversations we had with the following experts who provided knowledge, guidance, and/or manuscript reviews, namely: Yann Avram, Brian Bengert, Lief Cox, Shane Evans, David Goldak, Bernhard Friedrichs, Graham Heinson, Alan Jones, Benjamin Lee, Jean Legault, Frank Morrison, Ransom Reddig, Naser Meqbel, Geoffrey Plastow, Terry Ritchie, Martyn Unsworth, John Vann, Ken Witherly, Chris Wijns, and Garnet Wood.

REFERENCES

Alembaugh, D., H. Huang, J. Livermore, and M.S. Velasco, 2016, Resistivity imaging in a fold and thrust belt using ZTEM and sparse MT data: First Break, 34, 4, 65-72.

Balch, S.J., 1999, Ni-Cu sulphide deposits with examples from Voisey's Bay, in C. Lowe, M.D. Thomas, and W.A. Morris, eds, Geophysics in Mineral Exploration: Fundamentals and Case Histories: Geological Association of Canada, Short Course Notes, 14, 21-40.

Balch, S.J., T.J. Crebs, A. King, and M. Verbiski, 1998, Geophysics of the Voisey's Bay Ni-Cu-Co Deposits: 68th Annual International Meeting, SEG, Expanded Abstracts, 784-787.

Becken M. and L.B. Pedersen, 2003, Transformation of VLF anomaly maps into apparent resistivity and phase: Geophysics 68, 497-505.

Bostick, F.X., Jr., 1986, Electromagnetic array profiling (EMAP): 56th Annual International Meeting, SEG, Expanded Abstracts EM2.1, 60-61.

Bournas, N. and D. Thomson, 2013, Delineation of a Porphyry Copper-Gold system using ORION 3D DCIP- MT and CSAMT surveys-Case history, the Santa Cecilia Deposit, Chile: Presented at the KEGS-PDAC Symposium.

Broughton, D.W. and M.W., 2002, Exploration History and Geology of the Kansanshi Cu(-Au) Deposit, Zambia: Society of Economic Geologists Special Publication 9, 141-153.

Broughton, D.W. and T. Rogers, 2010, Discovery of the Kamoa Copper Deposit, Central African Copperbelt, D.R.C.: Society of Economic Geologists Special Publication 15, 287-297.

Burge, C., 2014, A new porphyry copper deposit at Cobre Panama project: Presented at PDAC Convention, Discoveries and Developments Session.

Caldwell, T.G., H.M. Bibby, and C. Brown, 2004, The magnetotelluric phase tensor: Geophysics Journal International, 158, 457–469.

Campanyà, J., J. Ledo, P. Queralt, A. Marcuello, and A.G. Jones, 2014, A new methodology to estimate magnetotelluric (MT) tensor relationships: estimation of local transfer-functions by combining inter-station transfer-functions (ELICIT): Geophysical Journal International, 198, 484–494.

Cagniard, L., 1953, Basic theory of the magnetotelluric method of geophysical prospecting: Geophysics, 18, 605-635.

Chave, A.D. and Jones, A.G. (Editors), 2012, The Magnetotelluric Method: Theory and Practice: Cambridge University Press.

Cifuentes, C., 2014, Aplicación de la Geofísica Aérea en la Exploración Minera: Presented at the 1st Chile Explore Congress.

Constable, S.C., R.L. Parker, and C.G. Constable, 1986, Occam's inversion: A practical algorithm for generating smooth models from electromagnetic sounding data: Geophysics, 52 (3), 289-300.

Craven, J.A., G. McNeice, B. Powell, R. Koch, I.R. Annesley, G. Wood, and J. Mwenifumbo, 2002, EXTECH IV Subproject 9T: A 3D audio-magnetotelluric survey at the McArthur River Mining Camp: Summary of Investigations 2002, Volume 2, Saskatchewan Geological Survey, Sask. Industry Resources, Misc. Rep. 2002-4.2, CD-ROM, Paper D-15, 6 p.

Cristall, J. and D. Brisbin, 2006, Geological sources of VTEM responses along the Collins Bay Fault, Athabasca Basin: Giant Uranium Deposits: Exploration Guidelines, Models, and Discovery Techniques Short Course, PDAC.

deGroot-Hedlin, C and S. Constable, 1990, Occam inversion to generate smooth, 2-dimensional models from magnetotelluric data: Geophysics, 55, 1613-1624.

deLugao, P.P. and P.E. Wannamaker, 1996, Calculating the two-dimensional magnetotelluric Jacobian in finite elements using reciprocity: Geophys. J. Int., 127, 806-810.

Dick, L.A., G. Ossandon, R.G. Fitch, C.M. Swift, and A. Watts, 1993, Discovery of blind copper mineralization at Collahuasi Chile, in S.B. Romberger and D.I. Fletcher, eds, Integrated methods in exploration and discovery: Society of Economic Geologists, Abstracts, AB 21-23.

Egbert, G.D, 1997, Robust multiple station magnetotelluric data processing: Geophys. J. Int., 130, 475-496.

Egbert, G.D. and A. Kelbert, 2012, Computational recipes for electromagnetic inverse problems: Geophys. J. Int., 189, 167–251.

Farquharson, C.G., D.W. Oldenburg, E. Haber, R. Shekhtman, 2002. An algorithm for the three-dimensional inversion of magnetotelluric data: 72nd Annual International Meeting of the Society of Exploration Geophysicists, 649–652.

Farquharson, C.G. and J.A. Craven, 2009, Three-dimensional inversion of magnetotelluric data for mineral exploration: An example from the McArthur River uranium deposit, Saskatchewan, Canada: Journal of Applied Geophysics, 68, 450–458.

Fayek, M. and K.K. Kyser, 1997, Characterization of multiple fluid events and rare-earth-element mobility associated with formation of unconformity-type uranium deposits in the Athabasca Basin, Saskatchewan: The Canadian Mineralogist, 35, 627-658.

FQML, 2017, Cobre Panama Reserves and Resources, http://www.first-quantum.com/Our-Business/Development-Projects/Cobre-Panama/Reserves-and-Resources/default.aspx, accessed May 01, 2017.

Fraser, D.C., 1969, Contouring of VLF-EM data: Geophysics, 34(6), 958-967.

Gandhi, S.S., 1995, An overview of the exploration history and genesis of Proterozoic uranium deposits in the Canadian Shield: Expl. And Res. for Atomic Minerals, 8, 1-47.

Griffin, W.L., G.C. Begg, and S.Y. O'Reilly, 2013, Continental-root control on the genesis of magmatic ore deposits: Nature Geoscience 6, 905–910

Goldak, D. and M. Goldak, 2001, Transient magnetotellurics with adaptive polarization stacking: 71st Annual International Meeting, SEG, Expanded Abstracts.

Gribenko, A. and M.S. Zhdanov, 2015, 3D inversion of regional MT data distorted by near-surface inhomogeneities using a complex distortion matrix: 85th Annual International Meeting, SEG, Expanded Abstracts.

Groom, R.W. and R.C. Bailey, 1989, Decomposition of magnetotelluric impedance tensors in the presence of local three-dimensional galvanic distortion: Journal of Geophysical Research, 94(B2), 1913-1925.

Gustafson, L.B. and J.P. Hunt, 1975, The porphyry copper deposit at El Salvador, Chile: Economic Geology, 70(5), 857-912.

Habashy, T.M., R.W. Groom, and B.R. Spies, 1993, Beyond the Born and Rytov approximations: A non-linear approach to electromagnetic scattering: Journal of Geophysical Research, 98(B2), 1759-1775.

Haber, E., E. Holtham, J. Granek, D. Marchant, D. Oldenburg, C. Schwarzbach, and R. Shekhtman, 2012, An adaptive mesh method for electromagnetic inverse problems: 82nd Annual International Meeting, SEG, Expanded Abstracts, 1–6.

Halley, S., Dilles, J.H., and Tosdal, R.M., 2015, Footprints: Hydrothermal alteration and geochemical dispersion around porphyry copper deposits: Society of Economic Geologists, SEG Newsletter, January 2015, 1-17.

Hehnke, C., G. Ballantyne, H. Martin, W. Hart, A. Schwarz, and H. Stein, 2012, Geology and Exploration Progress at the Resolution Porphyry Cu-Mo Deposit, Arizona: Society of Economic Geologists Special Publication 16, 147-166.

Heinson G.S., N.G. Direen, and R.M. Gill, 2006, Magnetotelluric evidence for a deep-crustal mineralizing system beneath the Olympic Dam iron oxide copper-gold deposit, southern Australia: Geology, 34(7), 573-576.

Heinson, G.S., S. Thiel, and P. Soeffky, 2016, Crust and mantle electrical resistivity heterogeneity: A vector to mineralisation?: Presented at the 23rd Electromagnetic Induction Workshop.

Hibbs, A., T. Petrov, J. Pedleton, S. Milberger, G. Eiskamp, and G.A. Wilson, 2012, New electromagnetic sensors for magnetotelluric and induced polarization geophysical surveys: 82nd Annual International Meeting, SEG, Extended Abstracts, 1-5.

Hitzman, M.W., D. Broughton, D. Selley, J. Woodhead, D. Wood, and S. Bull, 2012, The Central African Copperbelt: Diverse Stratigraphic, Structural, and Temporal Settings in the World's Largest Sedimentary Copper District: Society of Economic Geologists Special Publication 16, 487-514.

Holliday, J.R. and D.R. Cooke, 2007, Advances in geological models and exploration methods for copper ± gold porphyry deposits, in B. Milkereit ed., Proceedings of Exploration 07, 791-809.

Holtham, E. and D.W. Oldenburg, 2008, Three- dimensional forward modelling and inversion of Z- TEM data: 78th Annual International Meeting, SEG, Expanded Abstracts, 564-568.

Holtham, E. and D.W. Oldenburg, 2010, Three-dimensional inversion of ZTEM data: Geophysical Journal International, 182, 168–182.

Holtham, E.M., 2012, 3D Inversion of Natural Source Electromagnetic Data: PhD thesis, The University of British Columbia.

Hoschke, T., 2001, Geophysics of Andean Porphyry and Epithermal Deposits: Ore Deposits of South America Short Course.

Hoschke, T., 2011, Geophysical signatures of copper-gold porphyry and epithermal gold deposits, and implications for exploration: ARC Centre of Excellence in Ore Deposits, University of Tasmania.

Jones, A.G., 1988, Static shift of magnetotelluric data and its removal in a sedimentary basin environment: Geophysics 53(7), 967-978.

Jones, A.G., 2011, Three-dimensional galvanic distortion of three-dimensional regional conductivity structures: Comment on "Three-dimensional joint inversion for magnetotelluric resistivity and static shift distributions in complex media" by Yutaka Sasaki and Max A. Meju: Journal of Geophysical Research, 116(B12104), 1-5.

Jones, A.G., 2017, Magnetotellurics: status quo and quo vadimus, in V. Tschirhart and M.D. Thomas, eds, Proceedings of Exploration 17, 139-158.

Karous, M. and S.E. Hjelt, 1983, Linear filtering of VLF dip-angle measurements: Geophysical Prospecting, 31(5), 782–794.

Kelbert, A., N. Meqbel, G.D. Egbert, and K. Tandon, 2014, ModEM: A Modular System for Inversion of Electromagnetic Geophysical Data: Computers & Geosciences, 66, 40-53.

Kerr, A., 2003, Voisey's Bay and the nickel potential of Labrador: A summary for the nonspecialist: Current Research (2003), Newfoundland Department of Mines and Energy Geological Survey, Report 03-1, 231-239.

Key, K. and J. Ovall, 2011, A parallel goal-oriented adaptive finite element method for 2.5-D electromagnetic modelling: Geophysical Journal International, 186(1), 137–154.

Key, K., 2012, Marine EM inversion using unstructured grids: a 2D parallel adaptive finite element algorithm: 82nd Annual International Meeting, SEG, Expanded Abstracts, 1–5.

Killeen, P., 2017, Mineral Exploration Trends and Developments in 2016, Advances in Geophysical Technology: published by The Northern Miner, March 2017.

King, A., 2007, Review of Geophysical Technology for Ni-Cu-PGE deposits, in B. Milkereit ed., Proceedings of Exploration 07, 647-645.

Kingman, J.E.E., J.G. Donohue, and T.J. Ritchie, 2007, Distributed acquisition in electrical geophysical systems, in B. Milkereit ed., Proceedings of Exploration 07, 425-432.

Kirchner, G. and B. Tan, 1994, Key Lake: The trail of its discovery: CIM Bulletin, 87, 982, 57-61

Kuzmin, P., B. Lo, and E. Morrison, 2005, Final report on modeling, interpretation methods and field trials of an existing prototype AFMAG system: Ontario Geological Survey, Miscellaneous Data Release 167.

Labson, V.F., A. Becker, H.F. Morrison, and U. Conti, 1985, Geophysical exploration with audiofrequency natural magnetic fields: Geophysics, 50, 656-664.

Lang, J.R. and M.J. Gregory, 2012, Magmatic-Hydrothermal-Structural Evolution of the Giant Pebble Porphyry Cu-Au-Mo Deposit with Implications for Exploration in Southwest Alaska: Society of Economic Geologists Special Publication 16, 167–185.

Larsen, J., R.L. Mackie, A. Manzella, A. Fiordelisi, and S. Rieven, 1996, Robust smooth magnetotelluric transfer functions: Geophysical Journal International, 124, 801–819.

Legault, J.M., H. Kumar, B. Milicevic, and P. Wannamaker, 2009, ZTEM tipper AFMAG and 2D Inversion results over an unconformity uranium target in northern Saskatchewan: 79th Annual International Meeting, SEG, Expanded Abstracts, 1277-1281.

Lee, B., 2015, Three-Dimensional Electromagnetic Imaging of Porphyry Copper Deposits with MT and ZTEM Data: MSc thesis, University of Alberta.

Lee, B., M. Unsworth, J. Hübert, J. Richards, J.M. Legault, 2017, 3-D joint Z-axis tipper electromagnetic and magnetotelluric inversion: a case study from the Morrison porphyry Cu-Au-Mo deposit, British Columbia, Canada: Geophysical Prospecting, doi:10.1111/1365-2478.12554.

Legault, J.M., C. Wijns, C. Izarra, and G. Plastow, 2016a, The Balboa ZTEM discovery: EAGE Workshop on Deep Mineral Exploration.

Legault, J.M., C. Wijns, C. Izarra, G. Plastow, 2016b, The Balboa ZTEM Cu-Mo-Au porphyry discovery at Cobre Panama: ASEG Extended Abstracts.

Leppin, M. and D. Goldak, 2005, Mapping deep sandstone alteration and basement conductors utilizing audio magnetotellurics: Exploration for uranium in the Virgin River area, Athabasca Basin, Saskatchewan, Canada: SEG Expanded Abstracts 24, 591-594.

Liu, L., J.P. Richards, R.A. Creaser, S.A. DuFrane, K. Muehlenbachs, and P.B. Larson, 2016, Geology and age of the Morrison porphyry Cu–Au–Mo deposit, Babine Lake area, British Columbia: Canadian Journal of Earth Sciences, 53(9), 950-978.

Lo, B., P. Kuzmin, and E. Morrison, 2006, Field Tests of Geotech's Airborne AFMAG EM System: ASEG Extended Abstracts 2006, 1-5.

Lo, B. and M. Zang, 2008, Numerical modeling of Z-TEM (airborne AFMAG) responses to guide exploration strategies: 78th Annual International Meeting, SEG, Expanded Abstracts, 1098-1102.

Lo, B., J. Legault, P. Kuzmin, and M. Combrink, 2009, Z-TEM (Airborne AFMAG) tests over unconformity uranium deposits: ASEG Extended Abstracts 2009, 1-6.

Lowell, J.D. and J.M. Guilbert, J.M., 1970, Lateral and vertical alteration-mineralization zoning in porphyry ore deposits: Economic Geology, 65, 373–408.

McCuaig, T.M. and J.M.A. Hronsky, 2014, The mineral system concept: The key to exploration targeting: Society of Economic Geologists, Special Paper 18, 153-175.

McMonnies, B. and V. Gerrie, 2007, Ground geophysics and borehole logging—a decade of improvements, in B. Milkereit ed., Proceedings of Exploration 07, 39−49.

Mendelsohn, F. (Editor), 1961, The Geology of the Northern Rhodesian Copperbelt: MacDonald.

Meqbel, N.M, G.D. Egbert, P.E. Wannamaker, A. Kelbert, and A. Schultz, 2014, Deep electrical resistivity structure of the northwestern U.S. derived from 3-D inversion of USArray magnetotelluric data: Earth and Planetary Science Letters, 402, 290-304.

Moreno, T. and W. Gibbons, (Editors), 2007, The Geology of Chile: The Geological Society.

Morrison, H.F. and E. Nichols, 1997, Mineral Exploration with Natural Electromagnetic Fields, in A.G. Gubbins ed., Proceedings of Exploration 97, 527-538.

Nelson, P.H. and G.D. Van Voorhis, 1983, Estimation of sulfide content from induced polarization data: Geophysics, 48(1), 62-75.

Paré, P. and J. Legault, 2010, Ground IP-Resistivity, and airborne Spectrem and helicopter ZTEM survey results over Pebble copper-moly-gold porphyry deposit, Alaska: 80th Annual International Meeting, SEG, Expanded Abstracts 2010, 1734-1738.

Paré, P., A.V. Gribenko, L.H. Cox, M. Čuma, G.A. Wilson, M.S. Zhdanov, J. Legault, J. Smit, and L. Polomé, 2012, 3D inversion of SPECTREM and ZTEM airborne electromagnetic data from the Pebble Cu–Au–Mo porphyry deposit, Alaska: Exploration Geophysics, 43, 104-115.

Pedersen, L.B., 1998, Tensor VLF measurements: Our first experiences: Exploration Geophysics, 29, 52-57.

Piña-Varas, P. and M. Dentith, 2016, Magnetotelluric Study Across the Capricorn Orogen: Presented at the CET Members' Day.

Perrson, L., M. Erlström, M. Bastini, and L.B. Pederson, 2008, Airborne VLF measurement over the island of Gotland, Sweden: Presented at the 5th International Conference on Airborne Electromagnetics.

Powell, B., G. Wood, and L. Bzdel, 2007, Advances in Geophysical Exploration for Uranium Deposits in the Athabasca Basin, in B. Milkereit ed., Proceedings of Exploration 07, 741-769.

Rikitake, T., 1950, Electromagnetic induction within the earth and its relation to the electrical state of the Earth's interior: Bulletin of the Earthquake Research Institute, University of Tokyo, 28, 263-283.

Rodi, W. and R.L. Mackie, 2001, Nonlinear conjugate gradients algorithm for 2D magnetotelluric inversion: Geophysics, 66, 1, 174 – 187.

Sasaki, Y., M.J. Yi, and J. Choi, 2014, 2D and 3D separate and joint inversion of airborne ZTEM and ground AMT data: Synthetic model studies: Journal of Applied Geophysics, 104**,** 149-155.

Sattel, D., K. Witherly, and M. Becken, 2010, A brief analysis of ZTEM data from the Forrestania test site, WA: ASEG Extended Abstracts 2010.

Sattel, D. and K. Witherly, 2012, An overview of ZTEM data interpretation tools: Geoscience Australia Record 2012/04.

Sattel, D. and K. Witherly, 2015, The 3D joint inversion of MT and ZTEM data: ASEG Extended Abstracts 2015.

Schiller, A. A. 1978. The History of Uranium Discoveries in Northern Saskatchewan in the Last Decade: Uranium Exploration Techniques: Proceedings of the Saskatchewan Geological Society Symposium, 11-18.

Sillitoe, R.H., 2010, Porphyry Copper Systems: Economic Geology, 105, 3-41.

Sillitoe, R.H., 2012, Copper Provinces: Society of Economic Geologists Special Publication 16, 1–18.

Simpson, F. and K. Bahr, 2005, Practical Magnetotellurics: Cambridge University Press.

Siripunvaraporn, W., G. Egbert, Y. Lenbury, and M. Uyeshima, 2005, Three-dimensional magnetotelluric inversion: data-space method: Physics of the Earth and Planetary Interiors, 150, 3 – 14.

Soeffky, P.E., G. Heinson, and S. Thiel, 2015, Lithospheric Electrical Resistivity Heterogeneity: A Vector to Mineralisation: Presented at the South Australian Exploration and Mining Conference.

Tikhonov, A.N., 1950, On the determination of electrical characteristics of deep layers of the Earth's crust (*in Russian*): Dokladi Akademii Nauk, SSSR, 73, 295-297.

Theil, S., G. Heinson, C. Mudge, P. Chandrasekhar, and B. Alexander, 2012, 3D magnetotelluric inversion using cloud computing, in R. Lane ed., Abstracts from the ASEG Natural Fields EM Forum 2012: Geoscience Australia Record 2012/04, 189-194.

Thiel, S., G. Heinson, A. Reid, and K. Robertson, K., 2016, Insights into lithospheric architecture, fertilisation and fluid pathways from AusLAMP MT: ASEG Extended Abstracts 2016.

Thomas, D., 2015, Proterozoic Unconformity Uranium Deposits: Presented at the SEG Uranium Deposits Workshop, Society of Economic Geologists Annual Meeting.

Thomson, S., D. Fountain, and T. Watts, 2007, Airborne Geophysics – Evolution and Revolution, in B. Milkereit ed., Proceedings of Exploration 07, 19-37.

Toro, J.C., J. Ortúzar, J. Zamorano, P. Cuadra, J. Hermosilla, and C. Spröhnle, 2012, Protracted magmatic-hydrothermal history of the Río Blanco - Los Bronces District, Central Chile: Development of world's greatest known concentration of copper: Society of Economic Geologists Special Publication 16, 105-126.

Tuncer, V., M.J. Unsworth, W. Siripunvaraporn, and J.A. Craven, 2006, Exploration for unconformity-type uranium deposits with audiomagnetotelluric data: a case study from the McArthur River Mine, Saskatchewan, Canada: Geophysics, 71, 201–209.

Unsworth, M.J., 2007, Magnetotellurics, in D Gubbins and E Herrero-Bervera eds., Encyclopaedia of Geomagnetism and Paleomagnetism, 670-673.

Unsworth, M.J., V. Tuncer, W. Siripunvaraporn, J.A. Craven, 2006, Exploration for unconformity uranium deposits with audiomagnetotellurics: 76th Annual International Meeting, SEG, Expanded Abstracts.

Vozoff, K., 1972, The magnetotelluric method in the exploration of sedimentary basins: Geophysics, 37, 98–141.

Wannamaker, P.E., G.W. Hohmann, and S.H. Ward, 1984, Magnetotelluric responses of three-dimensional bodies in layered earths, Geophysics, 49(9), 1517-1533.

Ward, S.H., 1959, AFMAG – airborne and ground: Geophysics, 24, 761-789.

Ward, S.H., 1960, AFMAG – a new airborne electromagnetic prospecting method: Transactions AIME 217: 333-342.

Wardrop, 2009, Morrison copper/gold project – Feasibility study NI 43-101 technical report: http://www.pacificbooker.com/pdf/090313-832a-43-101_Final_Report.pdf, accessed on May 07, 2017.

Watts, M.D. and S.J. Balch, 2000, AEM-constrained 2D inversion of AMT data over the Voisey's Bay massive sulfide body, Labrador: SEG 2000 Expanded Abstracts.

Watts, A.H., 2002, Discovery of the Ujina Cu deposit, Collahuasi District, Chile: 72nd Annual International Meeting, SEG, Expanded Abstracts.

Wijns, C., 2013, Looking for graphite to find copper: geophysical exploration in Zambia: KEGS Symposium 2013 "Copper: Discovery and Delineation" Toronto, Canada - March 2nd, 2013.

Wijns, C., 2014, Looking for graphite and granite to find copper in Zambia: Presented at the ASEG WA Technical Night.

Witherly, K., 2002, The Application of Airborne EM to Porphyry Copper Exploration: Condor Consulting unpublished report.

Witherly, K., 2014, Geophysical Expressions of Ore Systems - Our Current Understanding: Society of Economic Geologists, Special Publication 18, 177–208.

Witherly, K., N. Pendrigh, J. Woodhead, and D. Sattel, 2016, Examples of ZTEM EM/mag over the Kemess (BC) and Resolution (AZ) Porphyry Copper Deposits: BCGS Fall 2016 Workshop.

Zhdanov, M.S., R.B. Smith, A. Gribenko, M. Čuma, and A.M. Green, 2011, Three-dimensional inversion of large-scale EarthScope magnetotelluric data based on the integral equation method – geoelectrical imaging of the Yellowstone conductive mantle plume: Geophysical Research Letters, 38, L08307.

Zhdanov, M.S., A. Gribenko, M. Čuma, and A.M. Green, 2012, Geoelectrical structure of the lithosphere and asthenosphere beneath the Northwestern United States: J. Geol. Geosci., 1 (2), 1000106, 1-6.

Zonge, K. and L.J. Hughes, 1991, Controlled Source Audio-Frequency Magnetotellurics: Electromagnetic Methods in Applied Geophysics: Society of Exploration Geophysicists, 713-810.